การจำลองแบบพลวัตเชิงโมเลกุลของการโตของผลึกแอลฟา-รีซอร์ซินอล

นายสมหวัง แซ่ตั้ง

วิทยานิพนธ์นี้เป็นส่วนหนึ่งของการศึกษาตามหลักสูตรปริญญาเภสัชศาสตรมหาบัณฑิต

สาขาวิชาเภสัชอุตสาหกรรม ภาควิชาวิทยาการเภสัชกรรมและเภสัชอุตสาหกรรม

คณะเภสัชศาสตร์ จุฬาลงกรณ์มหาวิทยาลัย

ปีการศึกษา 2556

MOLECULAR DYNAMICS SIMULATION OF α-RESORCINOL CRYSTAL GROWTH

Mr. Somwang Sae-tang

A Thesis Submitted in Partial Fulfillment of the Requirements

for the Degree of Master of Science in Pharmacy Program in Industrial Pharmacy

Department of Pharmaceutics and Industrial Pharmacy

Faculty of Pharmaceutical Sciences

Chulalongkorn University

Academic Year 2013

Thesis Title	MOLECULAR DYNAMICS SIMULATION OF α-RESORCINOL CRYSTAL GROWTH
By	Mr. Somwang Sae-tang
Field of Study	Industrial Pharmacy
Thesis Advisor	Jittima Chatchawalsaisin, Ph.D.
Thesis Co-advisor	Professor Jamshed Anwar, Ph.D.
	John Kendrick, Ph.D.

Accepted by the Faculty of Pharmaceutical Sciences, Chulalongkorn University in Partial Fulfillment of the Requirements for the Master's Degree

……. Dean of the Faculty of Pharmaceutical Sciences

(Assistant Professor Rungpetch Sakulbumrungsil, Ph.D.)

THESIS COMMITTEE

…….. Chairman

(Associate Professor Parkpoom Tengamnuay, Ph.D.)

…….. Thesis Advisor

(Jittima Chatchawalsaisin, Ph.D.)

…….. Thesis Co-Advisor

(Professor Jamshed Anwar, Ph.D.)

…….. Thesis Co-Advisor

(John Kendrick, Ph.D.)

…….. Examiner

(Narueporn Sutanthavibul, Ph.D.)

…….. Examiner

(Vorasit Vongsutilers, Ph.D.)

…….. External Examiner

(Assistant Professor Sujimon Tunvichien, Ph.D.)

สมหวัง แซ่ตั้ง: การจำลองแบบพลวัตเชิงโมเลกุลของการโตของผลึกแอลฟา-รีซอร์ซินอล (MOLECULAR DYNAMICS SIMULATION OF α-RESORCINOL CRYSTAL GROWTH) อ.ที่ปรึกษาวิทยานิพนธ์หลัก: อ. ภญ. ดร.จิตติมา ชัชวาลย์สายสินธ์, อ.ที่ปรึกษาวิทยานิพนธ์ร่วม: PROF. JAMSHED ANWAR, Ph.D., JOHN KENDRICK. Ph.D., 122 หน้า.

ผลึกของแอลฟา-รีซอร์ซินอลแสดงความไม่สมมาตรในการโตของผลึกทั้งจากสภาพสารละลายและสภาพไอ และขณะเกิดการละลายของผลึก คือหน้าผลึกทั้งสองหน้าที่อยู่ที่ปลายของแกนที่มีขั้วจะมีการโตหรือการละลายด้วยอัตราเร็วที่แตกต่างกัน จึงนำการจำลองแบบพลวัติเชิงโมเลกุลมาใช้เพื่อให้เข้าใจถึงพฤติกรรมที่ไม่ปกติในการละลายและการโตของผลึกแอลฟา-รีซอร์ซินอลบนหน้าผลึก $(0\bar{1}\bar{1})$ และ $(01\bar{1})$ โดยทำการศึกษา 4 แบบ ได้แก่ (1) การละลายของแอลฟา-รีซอร์ซินอลในน้ำที่อุณหภูมิต่าง ๆ (2) การโตของผลึกจากสารละลายอิ่มตัวยิ่งยวด3 ระดับ (3) การโตของผลึกจากสภาพไอ และ (4) การโตของผลึกจากสภาพหลอมเหลวที่อุณหภูมิต่างๆ ผลการศึกษาพบว่าอัตราการละลายและการโตของผลึกเร็วกว่าบนหน้าผลึก $(0\bar{1}\bar{1})$ ซึ่งเป็นหน้าผลึกที่มีขั้ว สอดคล้องกับผลที่สังเกตจากการทดลอง การละลายและการโตของผลึกเกิดขึ้นชัดเจนที่อุณหภูมิสูงกว่าซึ่งโมเลกุลมีพลังงานสูงและสามารถแพร่ได้รวดเร็วกว่า อย่างไรก็ตามอุณหภูมิที่สูงเกินไปจะส่งผลให้เกิดการจัดเรียงตัวใหม่ที่ผิวหน้าผลึกในการจำลองการโตของผลึกจากสภาพไอ นอกจากนี้ยังพบว่าระดับความอิ่มตัวยิ่งยวดมีอิทธิพลต่อการโตของผลึกในสารละลาย ระดับความอิ่มตัวยิ่งยวดที่สูงกว่าทำให้อัตราการโตเร็วกว่าตามที่คาดหมาย โดยเฉพาะที่บริเวณหน้าผลึก $(0\bar{1}\bar{1})$ การจำลองแสดงพฤติกรรมที่ชัดเจนของโมเลกุลที่ส่งผลต่อความไม่สมมาตรในการโตและการละลายของผลึก แต่สาเหตุของพฤติกรรมดังกล่าวยังไม่ชัดเจน ทั้งนี้ในกรณีของการละลายและการโตของผลึกจากสารละลาย น้ำ (ตัวทำละลาย) อาจมีบทบาทสำคัญในการกำหนดอัตราการละลายและการโตที่ผิวหน้าผลึก

ภาควิชา..วิทยาการเภสัชกรรมและเภสัชอุตสาหกรรม.. ลายมือชื่อนิสิต.....

สาขาวิชา..เภสัชอุตสาหกรรม..... ลายมือชื่อ อ.ที่ปรึกษาวิทยานิพนธ์หลัก.....

ปีการศึกษา.....2556..... ลายมือชื่อ อ.ที่ปรึกษาวิทยานิพนธ์ร่วม.....

ลายมือชื่อ อ.ที่ปรึกษาวิทยานิพนธ์ร่วม.….....

5276618033: MAJOR INDUSTRIAL PHARMACY
KEYWORDS: α-RESORCINOL/ MOLECULAR DYNAMICS SIMULATION/ DISSOLUTION/ CRYSTAL GROWTH/ SOLUTION/ VAPOUR/ MELT

SOMWANG SAE-TANG: MOLECULAR DYNAMICS SIMULATION OF α-RESORCINOL CRYSTAL GROWTH. ADVISOR: JITTIMA CHATCHAWALSAISIN, Ph.D., CO-ADVISORS: PROF. JAMSHED ANWAR, Ph.D., JOHN KENDRICK, Ph.D., 122 pp.

Crystals of α-resorcinol exhibit asymmetry during crystal growth, both from vapour and solution, and dissolution, that is, the two faces at the ends of the polar axis grow or dissolve at different rates. Molecular dynamics (MD) simulations were carried out to understand this extra-ordinary behavior of α-resorcinol in terms of dissolution and growth on $(0\bar{1}\bar{1})$ and (011) faces. Four investigations were carried out: (i) dissolution of α-resorcinol in water at a number of temperatures; (ii) crystal growth from solutions at three supersaturation levels; (iii) crystal growth from vapour and (iv) crystal growth from melt at various temperatures. The results showed that dissolution and crystal growth rates were faster on the $(0\bar{1}\bar{1})$ face, the polar face, which is consistent with experimental observations. The dissolution and crystal growth were more marked at higher temperatures where the molecules have higher energy and able to diffuse much more rapidly. However, too high a temperature caused surface reconstruction in the simulation of crystal growth from vapour. The supersaturation levels influenced the crystal growth in solution. The higher supersaturation level caused faster growth rate as expected, in particular on the $(0\bar{1}\bar{1})$ face. The simulations clearly reveal the distinct molecular behavior of the molecules that gives rise to the asymmetry in crystal growth and dissolution. However, it is not apparent as to what exactly is the origin of the behavior. For dissolution and crystal growth from solution, the water (solvent) may have a preferential role in deciding the relative dissolution rate and growth at the respective surfaces.

Department: Pharmaceutics and Industrial Pharmacy Student's Signature .....

Field of Study: Industrial Pharmacy Advisor's Signature .....

Academic Year: 2013 Co-advisor's Signature .....

Co-advisor's Signature .....

ACKNOWLEDGEMENTS

As lots of ingredients in any pharmaceutical formulation, my complete thesis also consists of a branch of knowledge which I have received from many important people. Clearly, this is the most favourite part of my thesis because I could describe what I cannot search some data from any journal but achieve them from very important people who I would like to express deep appreciation to them.

First of all, I would like to sincerely thank my supervisors: (i) Dr. Jittima Chatchawalsaisin for the memorable opportunity and series of discussion; (ii) Dr. John Kendrick for his variety of knowledge and languages, also his unforgettable help; (iii) Prof. Jamshed Anwar for his academic inspiration and work-life balance; (iv) Dr. Victoria Pennington for her computational technique and natural living concept; (v) Committee for suggestions, especially Dr. Narueporn Sutanthavibul for her kindness.

Moreover, Lots of friends are also my very special people, so I would like to thank all of them undoubtedly: (i) my colleague, especially Dr. Stephen Chan, for his kindly collaboration; (ii) my international friends for the fulfilled student's life; (iii) Thai friends for the large impact on my thesis and life diary.

I would like to thank British Council (PMI 2 Connect – Research Co-operation Award) for financial support in UK. Also thanks to IPI (University of Bradford) and CU.D.HIP for computational facilities. Finally, I would like to supremely thank my really most important parents, brother, sisters, and cousins for everything since I was born.

CONTENTS

Page

Page

LIST OF FIGURES

Figure **Page**

Figure **Page**

Figure **Page**

Figure **Page**

CHAPTER I

INTRODUCTION

Active pharmaceutical ingredients (APIs) are generally presented in their solid, crystalline form in drug formulations. This is because, crystals when formed tend to exclude impurities and hence crystallization can serve to purify the API and also because the solid state has lower rates of degradation and therefore greater stability. In the pharmaceutical industry, the choice of crystal structure, morphology, and particle size is important because it can have an impact on the manufacturing process, the stability of the product, and its bioavailability. Therefore, understanding the behavior of crystals, including how they grow, can be a guide towards development of the final product with desired properties.

Crystal growth is the formation process of the crystalline solid form from solution, vapour, or melt (Wahab, 2009). In an industrial context, crystal growth from solution and melt are the usual crystallizing methods (Scheel, 2000). Crystal growth from solution occurs when dissolved solute elements in supersaturated solution are slowly precipitated from a saturated solution. Whilst, crystal growth from the melt occurs when a molten material is cooled down until it crystallizes. The objective of all crystal growth processes is to produce a crystalline solid which has the desired properties. These properties include purity, size, and crystal morphology.

Computer simulation is a tool to study macroscopic systems such as crystal growth process by performing simulations of microscopic models. The model results are compared with theoretical and experimental data to evaluate the accuracy of the model.

As a result, computer simulations can used to confirm the experimental data, guide further experiments, and study systems which are inaccessible by experiments.

Molecular dynamics (MD) simulation is a particular computer simulation method which reveals the dynamic behavior of molecules in a system. The forces between atoms and molecules are calculated using a forcefield, and employed by the MD algorithm to simulate the behavior of the system as a function of time. The accuracy of the calculations depend on the limitations of computers such as computer memory, speed, and precision. (Allen and Tildesley, 1987). These simulations reveal how the molecules interact and behave in the studied system.

Crystals of polar molecules such as resorcinol are of interest because of their unidirectional growth along the polar axis. α-Resorcinol has a simple structure and its crystals grow asymmetrically. Consequently, it has been used as a model for investigating the effects of solvents and additives (Wells, 1949; Wireko et al., 1987; Davey et al., 1988) in crystal growth and dissolution processes. In spite of a number of studies, understanding of the mechanisms of crystal growth and dissolution processes is still not complete. The experimental studies include studies of crystal growth from solution (Wells, 1949; Wireko et al., 1987; Davey et al., 1988) and vapour (Srinivasan and Sherwood, 2005; Srinivasan and Sherwood, 2011), while the simulation studies have been used to investigate the mechanism for the crystal growth from solution on crystal surfaces as a function of temperature (Hussain and Anwar, 1999) and vapour (Weissbuch et al., 2006; Anwar et al., 2007).

In this study, MD simulations were conducted to study the effect of water on the dissolution of α-resorcinol crystal in water at three different temperatures. For

crystal growth, MD simulations were performed to study the growth in different states: solution, vapour, and melt. From solution, the effect of three levels of supersaturation was studied. From vapour and melt, the effect of four temperatures on the crystal growth was investigated. The MD trajectories and the density profiles of solvent and solute were used to discuss the behavior of crystal dissolution and growth.

Objectives of the present study

1. To investigate the crystal growth of α-resorcinol crystals grown from supersaturated solutions, vapour, and melt by MD simulations
2. To study dissolution of α-resorcinol crystal by MD simulation

CHAPTER II

LITERATURE REVIEW

2.1 α-Resorcinol

Resorcinol, 1, 3-dihydroxybenzene, is a white crystal (α-resorcinol) with weak odour and bittersweet taste (Schmiedel and Decker, 2000). It has been used in human medicine as an antiseptic and in keratolytic topical medications at low concentrations of 1–2%. Sometimes much higher concentrations (up to 50%) have been used in peeling agents or in pastes for the treatment of leg ulcers (Hahn, 2006). The molecular mass of resorcinol is 110.11 and the chemical formula is $C_6H_6O_2$. Its structure is composed of a phenol structure and a substitution of hydroxyl group for a hydrogen atom in the meta position (Hahn et al., 2006).

Resorcinol can crystallise in two polymorphs (Kofler, 1943). α-Resorcinol is the polymorph in which both hydroxyl groups arrange in the same direction, whilst β-resorcinol possesses opposite arrangement of both hydroxyl groups (Figure 2.1). α-Resorcinol is stable at ambient temperature and pressure, and can transform to β-resorcinol when the temperature is above 347 K at ambient pressure (Yoshino et al., 1999) or at a pressure of 5 kbar at ambient temperature (Sharma et al., 1985). Both polymorphs crystallize in the $Pna2_1$ space group. The α polymorph has the lower density (1.278 g/cm3 at 20 °C (Schmiedel & Decker, 2000).

Resorcinol molecules are polar and in the α-resorcinol crystal have a high dipole moment due to the position of the hydroxyl groups on the benzene ring. Normally, α-

resorcinol crystals grow asymmetrically along the polar direction. The α-resorcinol crystals have 2 interesting faces that terminate the polar axis. The polar face, $(0\bar{1}\bar{1})$, is rich in hydroxyl groups and the non-polar face, (011), is rich in benzene rings, as shown in Figure 2.2. Due to the simplicity of the α-resorcinol structure and its asymmetric growth, it has been used as a model drug in the study of behavior of crystal growth (Wells, 1949).

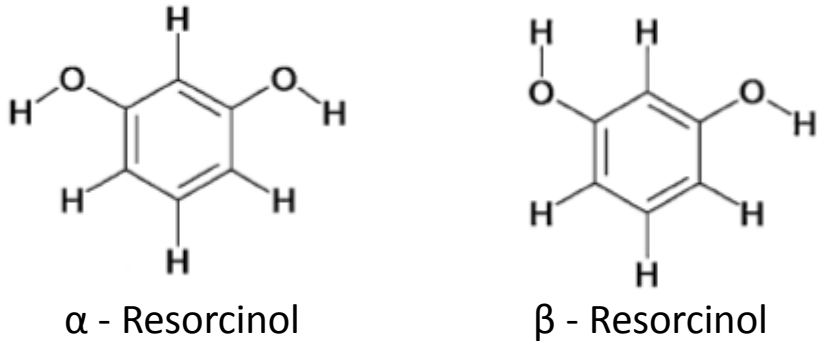

Figure 2.1 Structures of α -resorcinol and β-resorcinol.

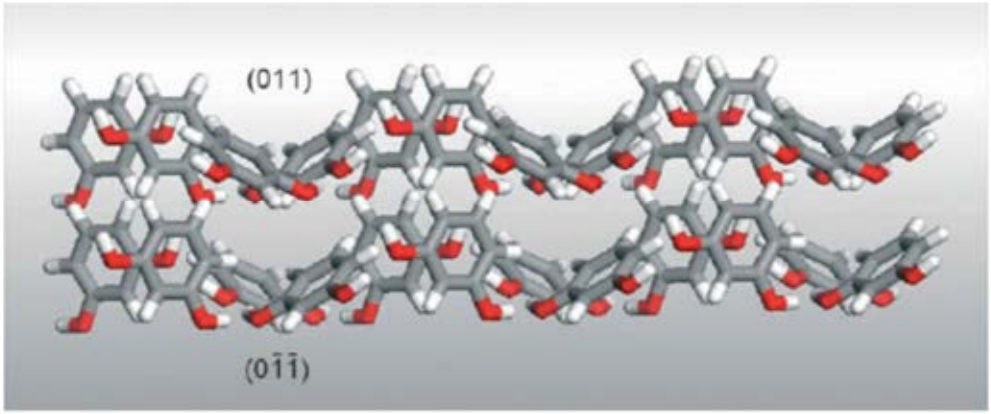

Figure 2.2 Molecular orientation at surfaces of α-resorcinol crystal where the $(0\bar{1}\bar{1})$ face is on the bottom and the (011) face is on the top of figure (Anwar et al., 2007).

2.2 Crystal growth

Crystal growth has been studied since the seventeenth century (Sunagawa, 2005) and first applied in an industrial context in 1902 (Scheel, 2000). Crystal growth can be obtained from vapour, melt, or solution (Wahab, 2009).

Crystals are mostly grown from solution. This occurs when the concentrations of the components in the crystal reach a certain level of supersaturation. When the solution reaches a certain level of saturation, the driving force in the supersaturate solution wants to expel the solute molecules and consequently the material forms crystals. The morphology of a crystal is determined by its crystal structure, and the crystal growth conditions and crystallization proceeds under the conditions. The internal crystal structure has been proven to affect the habit of crystalline materials (Hartman and Bennema, 1980). The crystal growth conditions such as solvents or additives, and process have been studied extensively as to how they can enhance or inhibit crystal growth and hence affect crystal morphology (Wireko et al., 1987; Weissbuch et al., 1995; Bhat and Dharmaprakash, 2002).

Many studies have been conducted to investigate the effects of solvent on crystal growth. Wells (1949) found that changing the solvents i.e. water, benzene, and ethyl acetate could affect the habit of the resorcinol crystal. The effect of changing solvents i.e. methanol, ethanol and water was also shown in l-pyroglutamic acid crystal growth (Wang et al., 1999). Moreover, the solvent can either inhibit or enhance the rate of growth of the crystal. It was postulated that the crystal growth inhibition was due to the strong adsorption of solvent at the crystal surface. In this case, the more

strongly bound of water at the non-polar, (011), face of α-resorcinol crystal caused the inhibition on this face (Wireko et al., 1987). This led to the observation that the (011) face grew slower than $(0\bar{1}\bar{1})$ face over a range of temperatures and supersaturations (Davey et al., 1988).

The solvent can enhance the crystal growth if the solvent molecules can be readily expelled/exchanged from the surface. Some complicated mechanisms have also been proposed. For example, the solvent may bind to the outermost layer of surface leaving cavities unfilled which can then be occupied by the solute. After that, the solute will then repel the solvent from the surface leading to the fast crystal growth by a kind of relay mechanism. For example, the (R, S)-alanine crystal grows differently on each face. The crystal has a polar morphology with the COO^- groups emerging at the flat-C face and NH_3^+ groups at the opposite face (Shimon et al., 1990). The face with carboxylate groups contains cavities and it grows and dissolves faster in aqueous solution than that of the smoother aminium ion face. It can be explained that water molecules were bound to the outermost layer, allowing the remaining portions of the surface to be relatively easily accessible to approach solute molecules, the solute NH_3^+ moiety, which then repels bound water molecules to develop the crystal.

The role played by "tailor-made" additives or impurities on crystal morphology has also been studied. Additives or impurities are often known to interact with the crystalline phase in the crystal growth process. For instance, they influence the nucleation and growth kinetics. An example is the effect of aspartic acid on crystal growth of α-glycine. Aspartic acid anions were found to selectively bind to the crystal faces of α-glycine and inhibit its growth (Poornachary et al., 2007). Similarly, solvents

can also play a tailor-made role. The bipyramidal morphology of α-rhamnose monohydrate obtained when it was grown from aqueous solutions were changed to a pyramidal crystals by the addition of methanol as a co-solvent (Shimon et al., 1990).

Without no solvent effect, the crystal growth from vapour phase has also been widely studied. The morphology of α-glycine crystals obtained by sublimation (Boek et al., 1991) was shown to be in good agreement with the theoretically predicted morphology of α-glycine (Berkovitch-Yellin, 1985). In case of α-resorcinol, the asymmetric growth from vapour along the polar direction was observed as the same behavior as the crystal growth from solution (Srinivasan and Sherwood, 2005).

2.3 Molecular dynamics simulations

Understanding the molecular mechanisms of crystal growth is an essential step toward controlling crystal growth, morphology and shape. Since crystal growth kinetics can be studied in a number of ways depending on the purpose and the scope of the investigation, it is useful to complement experimental and analytical studies by using molecular level computations because they can identify specific molecular mechanisms as well as to uncover details that are not always accessible in physical experiments. That is to say the computational studies such as molecular dynamics (MD) simulation can make predictions and offer guidance prior to further experimental studies.

MD simulations reveal the dynamical behavior of molecules in a system by calculating the interaction forces between the molecules using the specified forcefield. The changes in positions and velocities of the molecules and atoms are then determined by integration Newton's laws of motion (Allen and Tildesley, 1987).

2.3.1 Molecular interactions

The energy and forces between atoms and molecules are calculated using the molecular mechanics method, which requires the specification of a force field. The force field is a set of parameters describing the molecular potential energy. It contains terms of both bonded and non-bonded energies for intramolecular and intermolecular forces, respectively. As a result, the potential energy, V_{total}, of a molecule is calculated by the sum of both energies as shown in Equation 2.1.

$$V_{total} = V_{bonded} + V_{non\text{-}bonded} \quad (2.1)$$

V_{bonded} is the sum of bonded interaction energies including bond stretching, bond angle bending, and twisting of torsions angles, while $V_{non\text{-}bonded}$ is the sum of van der Waals interaction (V_{vdW}) and electrostatic interaction (V_{elec}) energies.

For bonded interaction energies, V_{bonded}, firstly, bond stretching interaction occurs between two atoms which are bonded to each other as shown in Figure 2.3. The energy of bond stretching interaction, $V_{Bond\ Stretching}$, is calculated by the Equation 2.2.

$$V_{Bond\ Stretching} = \frac{1}{2} k_l (l - l_0)^2 \quad (2.2)$$

where k_l is the bond stretching constant, l is the bond length, and l_0 is the equilibrium length for a given bond.

Secondly, angle bending interaction occurs among three atoms when two atoms bond to the same center atom and create an angle between the two bonded as shown in

Figure 2.3. The energy of angle bending interaction, $V_{Angle\ Bending}$, is calculated by the Equation 2.3.

$$V_{Angle\ Bending} = \frac{1}{2}\, k_\theta(\theta - \theta_0)^2 \qquad (2.3)$$

where k_θ is the angle bending constant, θ is the angle between three bonded atoms, and θ_0 is the equilibrium bond angle.

Lastly, torsional angle interaction occurs when the two groups of atoms bonded to the center bond and one of them rotates around the bond as shown in Figure 2.3. The energy of torsional angle interaction, $V_{Torsional\ angle}$, is calculated by Equation 2.4:

$$V_{Torsional\ angle} = \frac{k_\phi}{2}\,[1 + \cos(n\phi - \gamma)] \qquad (2.4)$$

where k_ϕ is the height torsional barrier, n is the periodicity, ϕ is the torsional angle, and γ is where the torsional angle pass through a minimum or maximum point of energy.

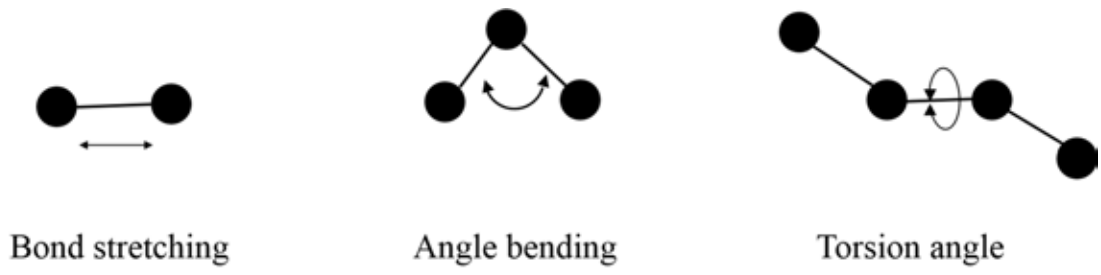

Figure 2.3 Schematic diagram of force field terms: bond stretching, angle bending, and torsional angle.

Besides bonded interactions, the non-bonded interactions are used to describe intermolecular forces between atoms which are not bonded together. The interactions consist of van de Waals interaction and electrostatic interaction.

van der Waals interaction is used to explain the attractive and repulsive forces between atoms which are not directly bonded. The van der Waals interaction between two atoms is often represented by the Lennard-Jones potential or by the Buckingham potential. The Lennard-Jones potential is widely used to represent the potential because of its simplicity and computational effective. It contains repulsive, $\left(\frac{\sigma}{r}\right)^{12}$ and attractive parts, $(\frac{\sigma}{r})^6$, where ε is the well depth of energy, σ is the diameter and r is the distance between atoms as described in the Equation 2.5.

$$V_{\text{Lennard-Jones}} = 4\varepsilon\{\left(\frac{\sigma}{r}\right)^{12} - (\frac{\sigma}{r})^6\} \quad (2.5)$$

For atoms between which the two parameters are not defined, the individual ε and σ values are used to calculate the atomic pair interactions. This is commonly done using the Lorentz-Berthelot mixing rules. Therefore the unknown ε and σ parameters between atoms are calculated in Equation 2.6 and 2.7.

$$\varepsilon_{ij} = \sqrt{\varepsilon_i \varepsilon_j} \quad (2.6)$$

$$\sigma_{ij} = \frac{1}{2}(\sigma_i + \sigma_j) \quad (2.7)$$

The Buckingham potential (Equation 2.8) is more accurate because it takes the form of realistic and exponential functions where A, ρ, and C are parameters in order to reproduce experimental data where $Ae^{(-r/\rho)}$ represents repulsive part and $\frac{C}{r^6}$ represents attractive part. The drawback of the Buckingham potential is that this potential becomes strongly negative at extremely short distances.

$$V_{\text{Buckingham}} = Ae^{(-r/\rho)} - \frac{C}{r^6} \quad (2.8)$$

In addition to van de Waals interactions, the electrostatic interactions represent a pair potential between atoms that have a partial for formal charge due to enhanced or reduced electron density around the atoms. The electrostatic interactions are calculated by using Coulomb's law which gives the electrostatic potential energy between two point charges as the Equation 2.9.

$$V_{coulombic} = \frac{Q_i Q_j}{4\pi\varepsilon_0 r_{ij}} \qquad (2.9)$$

where $Q_i \; and \; Q_j$ are the charges of atom i and j, respectively, ε_0 is the dielectric constant, and r_{ij} is the distance between two atoms. (Cornell et al., 1995)

2.3.2 Practical aspects of computer simulations

Periodic boundary conditions

Periodic boundary condition (Born and von Kármán, 1912) is an inventive method that counteracts a limitation of the simulation of finite models which has a boundary effect at the edges of simulation box. The condition completely eliminates the influence of the edges of simulation box and produces an infinite system of interacting particles.

A periodic system is generated by replicating a central cell in all directions (x, y and z) as shown in Figure 2.4. In this way, an infinite macroscopic system is produced but only the particles in the central cell need to be considered as independent. If a particle moves out of the central box, it will immediately be replaced with an image of itself from the opposite side of the box. Thus, the edges of box are eliminated and the number of particles in the central box is still conserved.

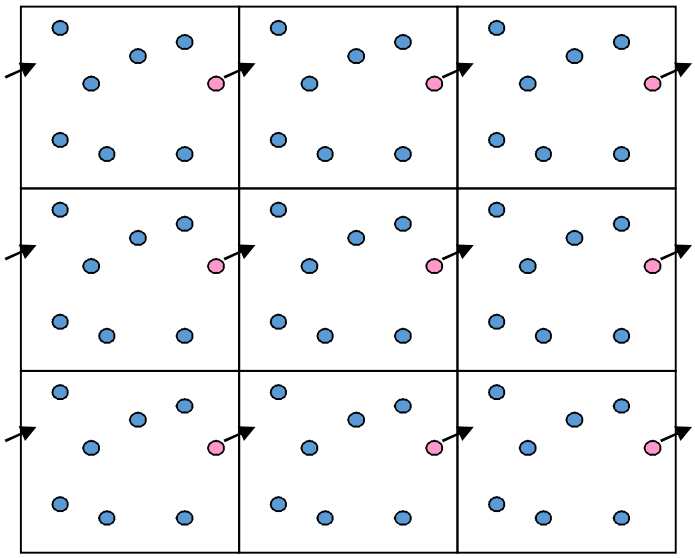

Figure 2.4 The periodic boundary condition.

Cutoff radius

According to the time consumption of the force calculation in a computer simulation, a cutoff radius can be set. Consequently, the energy contributions between two particles whose inter-particulate distance lies beyond the cutoff are not calculated and set to zero. In general, the cutoff radius is set for the short-range interaction; the energy quickly drops to zero where the distance is far beyond the cutoff radius. However, the use of cutoff radius can cause an abruption in force if the long-range forces decay slowly as a function of distance such as coulombic forces. In other words, there can be a relatively large discontinuity in force when two particles move away from or towards each other across the cutoff radius leading to poor energy conservation with small cutoff radius in particular.

Long-range interactions

Since there is a discontinuity in force for long-range interactions if the cutoff radius is very short, a number of methods have been developed to address this problem. The Ewald summation (Ewald, 1921) solves this problem by calculating the interactions of all particles in the central cell with their images in the periodic cells. The Ewald summation is also adapted to improve the progression of calculation such as smoothed particle-mesh Ewald (SPME) method (Essmann et al., 1995). Furthermore, the shifted potential (Allen and Tildesley, 1987) is also a good technique for rough approximation to shift the potential of the interaction far beyond the cutoff to reach zero at the cutoff radius.

2.3.3 Basic steps in molecular dynamics simulations

Firstly, the positions and velocities of particles set up in the initial system for MD simulation are obtained from crystallographic data. Secondly, the system is equilibrated to reduce the probability of localized fluctuations in the energy by adjusting the temperature and rescaling velocities. After that, the simulation is continued and the trajectories of the system are calculated and generated which then analyzed for the physical properties.

2.3.4 Applications of MD simulations

MD simulations are applied to reveal pharmaceutical industrial aspects of interest, especially in crystal growth. The MD simulations are performed to understand the crystal growth and dissolution phenomena by comparing with experimental data or to guide further crystal development such as optimization of the conditions for

individual crystal growth. Mainly, the studies focused on the mechanisms of dissolution and growth of crystals in solution (Hussain and Anwar, 1999; de Leeuw, 2002; Piana and Gale, 2005; Yang et al., 2006) and vapour phase (Weissbuch et al., 2006; Anwar et al., 2007).

In cases of crystal growth in solution, MD simulations have been applied to study the mechanism of solvent effect on crystal growth. The dissolution and growth of surfaces in [001] and [00$\bar{1}$] directions of urea crystal in contact with aqueous solution was studied (Piana and Gale, 2005). The dissolution and growth of the single surface were found to occur rapidly. It was also shown that the removal of surface layer defects was the rate-limiting step for crystallization. A barrier due to water molecules on the surface must be removed before the urea molecules were adsorbed to complete the layer (Piana and Gale, 2005).

For α-resorcinol, the study on the (0$\bar{1}\bar{1}$) and (011) interfaces of α-resorcinol crystal with water provided a detailed picture of both the dynamics and energetics of water interaction at the two faces. The diffusion of water molecules was characterized in the surface layer by diffusion constants from which the lower diffusion constant represented stronger adsorption of water molecules to the crystal surface. In addition, the higher affinity of water for the crystal surface was identified by the lower crystal-water binding energies. The results from the molecular dynamic simulations of the (0$\bar{1}\bar{1}$) and (011) crystal water interface showed the stronger adsorption of water at the slower growing (011) face, by the lower diffusion rates of water molecules and the lower average crystal-water binding energies (Hussain and Anwar, 1999).

The study of crystal growth from vapor phase is a way to exclude solvent effect on crystal growth. The crystal growth from vapor could be a two-step process: adsorption of molecule at the surface, followed by reorientation and integration. For instance, self-poisoning was a reasonable mechanism to explain the unidirectional growth of α-resorcinol in the vapor phase (Weissbuch et al., 2006). Self-poisoning was the mechanism that suggested a misdocking of α-resorcinol molecules at the slow growing face. The α-resorcinol molecule preferred to misdock into the site at (011) face because of gaining more layer energy, ΔE_l, the energy released when a new layer was formed. In contrast, α-resorcinol molecule cannot misdock into any site at $(0\bar{1}\bar{1})$ face since the penalty in layer energy was high. Therefore, the $(0\bar{1}\bar{1})$ face of resorcinol crystal could grow more than the (011) face (Weissbuch et al., 2006). The molecular density of α-resorcinol could display disordered $(0\bar{1}\bar{1})$ and (011) faces. The $(0\bar{1}\bar{1})$ face was observed to have a minimal surface reconstruction and the topmost layer was essentially crystalline, while the topmost layer and parts of the second layer of (011) face were highly disordered or effectively molten (Anwar et al., 2007).

CHAPTER III

METHODS

3.1 Force fields

Molecular dynamics simulations were performed using the molecular dynamics (MD) simulation package, DL_POLY package version 2.2 (Smith et al., 2005), using the optimized AMBER force field parameters (Cornell et al., 1995; Chatchawalsaisin et al., 2008) of α-resorcinol (1, 3-benzenediol) molecules. For water molecules, the TIP4P model was selected because it has been parameterized for simulation of liquid water. The TIP4P water force field (Hernandes et al., 2003) was employed for the solvent molecule in the simulation. The molecular structure of α-resorcinol is shown in Figure 3.1 and that of TIP4P water is shown in Figure 3.2.

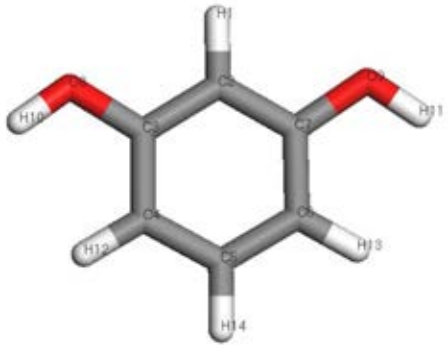

Figure 3.1 Molecular structure of α-resorcinol by Material studio version 5.5.

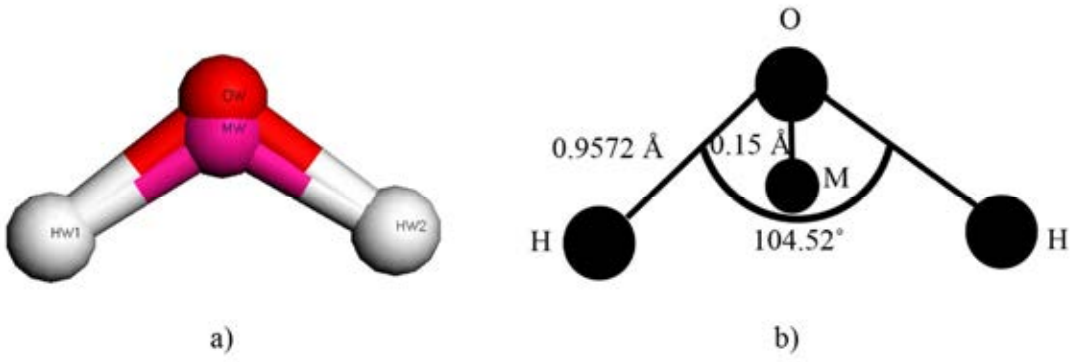

Figure 3.2 a) Molecular structure of TIP4P water generated by Material studio version 5.5 and b) The values of TIP4P structure (Jorgensen et al., 1983).

3.2 Force field verification

The force field used for the resorcinol molecule is based on the AMBER force field and had been further optimized to reproduce the bulk properties of the two polymorphs of resorcinol (Chatchawalsaisin et al., 2008). Prior to the simulation, the force field of TI4P water molecule was verified by determination of water density at varied temperatures in MD simulations using the procedure outlined below.

A 22 x 22 x 22 angstrom^3 cubic box was generated and 343 water molecules were inserted into the box by GROMACS version 3.2 (Van der Spoel et al., 2004). MD simulations under three-dimensional periodic boundary conditions were performed with the constant temperature and pressure (NPT) ensemble, using DL_POLY package version 2.2. Nosé-Hoover thermostat (Hoover, 1985) and barostat (Melchionna et al., 1993) with relaxation times of 0.1 and 1.0 ps, respectively, were used to control

temperature and pressure at 1 atm. The Ewald summation method (Hoover, 1985) was used to calculate long range electrostatic interaction with a relative error of 10^{-6}. All bonds were constrained using the SHAKE algorithm (Ryckaert et al., 1977). The time step was 0.002 ps and the cutoff radius of non-bonded interaction which limits calculation of the interaction between molecules, was 10 angstrom.

The simulations were carried out at different temperatures: 283, 293, 303, 313, 323, 333, 343, 353, and 363 K for 100 ps. The average densities during constant volume period of these simulations during the last 70 ps were interpolated to compare with the experimental density profiles of water (Kell, 1975).

3.3 Molecular dynamics simulations

3.3.1 Dissolution

A 42 x 46 x 150 angstrom^3 simulation cell was generated by GROMACS version 3.2 consisting of a crystal slab of α-resorcinol containing 768 molecules with the non-polar face, (011), and the polar face, $(0\bar{1}\bar{1})$, exposed to 3200 water molecules as shown in Figure 3.3. The MD simulations were performed under three-dimensional periodic boundary using DL_POLY package version 2.2 with a constant temperature and constant stress (NST) ensemble but with the simulation cell angles remaining fixed, coupled to Nosé-Hoover thermostat and barostat with relaxation times of 0.1 and 1.0 ps, respectively, to control temperatures and pressure (1 atm). The smooth particle mesh Ewald (SPME) method (Essmann et al., 1995) was used to calculate long range electrostatic interaction with a relative error of 10^{-5}. All bonds were constrained using the SHAKE algorithm. The time step was 0.002 ps and the non-bonded interaction

cutoff radius, which limits calculation of the interaction between molecules, was 12 angstrom.

The systems were first equilibrated for 500 ps at 3 different temperatures, 200, 250, and 300 K, with an increased mass for the resorcinol molecules (100 fold higher) in the force field input. The increased mass maintained the integrity of the crystals while allowing the water molecules to equilibrate about the exposed crystal faces. The different temperatures were employed to generate different starting positions of the water molecules. After equilibrating for 500 ps, the crystal slab and water layer thickness were approximately 60 and 50 angstrom, respectively.

The 200K equilibrated box was used as a starting configuration for simulations at 293, 313, and 333 K. In order to remove any bias resulting from the starting configuration, three simulations were also carried out at 333 K using the boxes equilibrated at 200, 250 and 300 K. All simulations were carried out for 15 ns, but the simulations carried out at 293 and 313 K were continued for further 50 ns. The schematic diagram showing the simulation of dissolution behavior of α-resorcinol is shown in Figure 3.4.

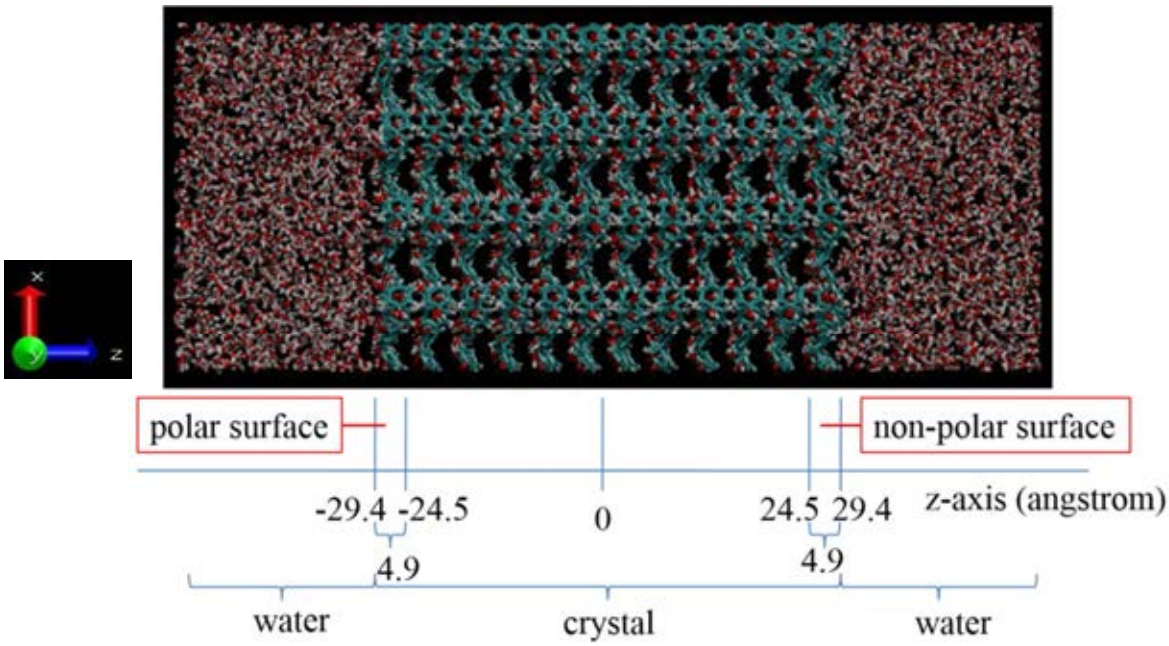

Figure 3.3 The 200 K equilibrated structure of α-resorcinol crystal and water used as the starting configuration for dissolution simulations. The non-polar face, (011), is on the right and the polar face, ($0\bar{1}\bar{1}$), is on the left.

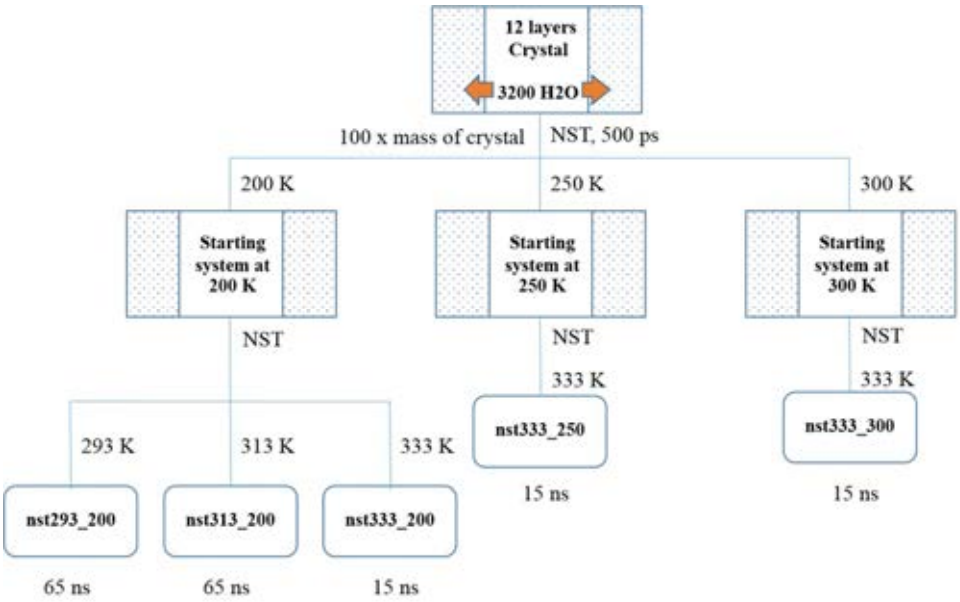

Figure 3.4 Schematic diagram showing the simulations of dissolution. H2O represents water molecule.

3.3.2 Crystal growth from solution

A 42 x 46 x 150 angstrom^3 cell generated by GROMACS version 3.2 consisted of a crystal slab of α-resorcinol containing 768 molecules with the non-polar face, (011), and the polar face, $(0\bar{1}\bar{1})$, exposed to 3 different supersaturated solutions of α-resorcinol in water at 293 K which higher ratio of α-resorcinol to water molecules represent more concentrated of resorcinol in solution. These ratios were 549:2122 (level of supersaturation, s = 1.1), 593:1850 (s = 1.3), and 631:1621 (s = 1.5), respectively. The 549:2122 system is shown in Figure 3.5. The simulations were performed in a constant temperature and constant stress ensemble (NST) under three-dimensional periodic boundary conditions. The Nosé-Hoover thermostat and barostat with relaxation times of 0.1 and 1.0 ps, respectively, were used to control temperature and pressure at 1 atm. The SPME method was used to calculate long range electrostatic interaction with a relative error of 10^{-5}. All bonds were constrained using the SHAKE algorithm. The time step was 0.002 ps and the interaction potential cutoff radius, which limits calculation of the interaction between molecules, was 12 angstrom.

The boxes were first equilibrated for 500 ps at 200 K. The highest supersaturated solution (631:1621) was also equilibrated at 250 and 300 K. An increased mass was assigned to the resorcinol molecules (100 fold higher) in the force field input. The increased mass maintained the integrity of the crystals while allowing the solution molecules to equilibrate about the exposed crystal faces. The different temperatures were employed to generate different starting positions of the solution molecules. After 500 ps, the crystal slab thickness was approximately 60 angstrom, whilst the solution layer was approximately 50 angstrom.

A total of five simulations with different equilibrated configurations were carried out at 293 K for 65 ns as shown Figure 3.6. Three replicate simulations using the highest level of supersaturated solution (631:1621) were carried out to remove any bias resulting from the starting configuration.

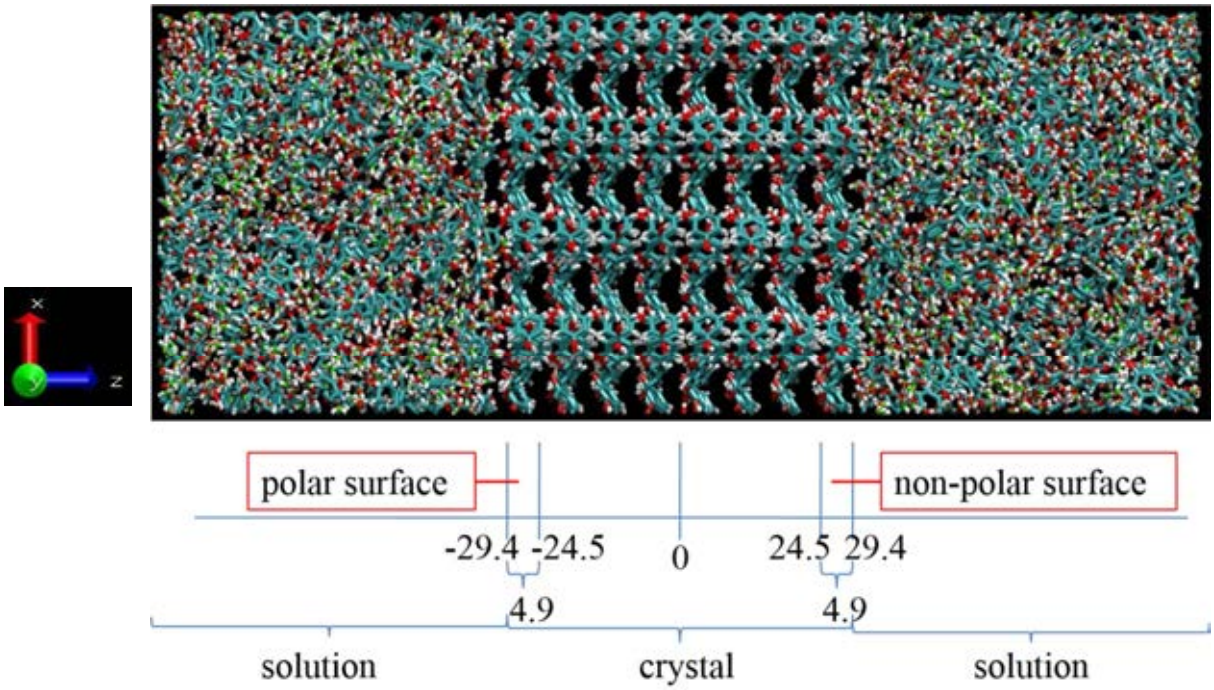

Figure 3.5 The 200 K equilibrated structure of α-resorcinol crystal and α-resorcinol in water solution (549:2122 ratio) used as starting configuration for simulating crystal growth from solution. The non-polar face, (011), is on the right and the polar face, $(0\bar{1}\bar{1})$, is on the left.

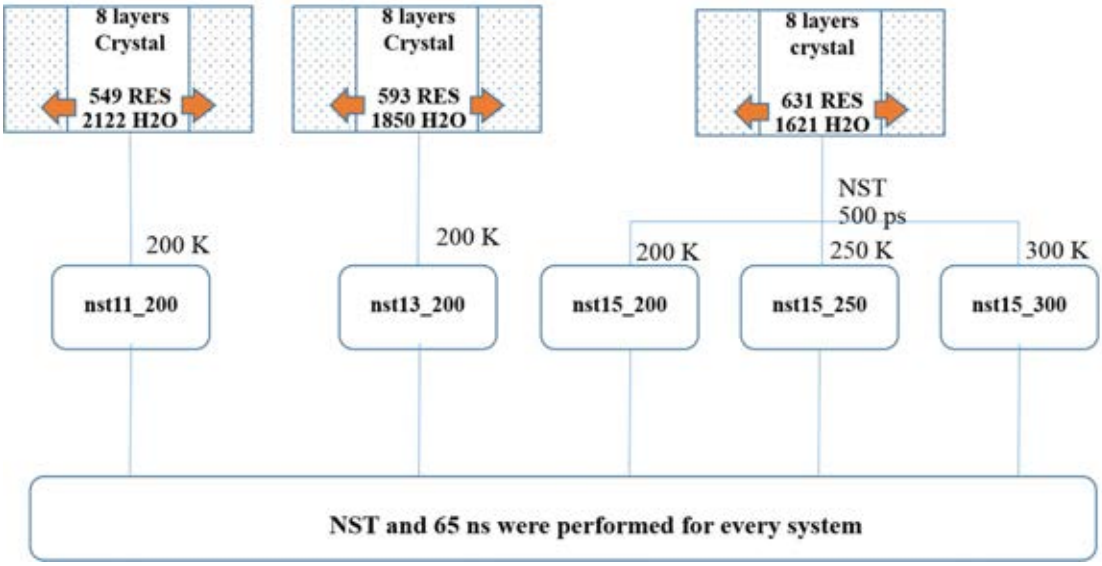

Figure 3.6 Schematic diagram showing the simulations of crystal growth from solution. RES and H2O represent α-resorcinol and water molecules in solution, respectively.

3.3.3 Crystal growth from vapour

A 85 x 92 x 220 angstrom^3 cell was generated by in-house programs (J. Anwar, University of Bradford) consisting of a α-resorcinol crystal slab containing 3072 molecules with the non-polar face, (011), and the polar face, $(0\bar{1}\bar{1})$, exposed to 1500 α-resorcinol molecules in vapour phase as shown in Figure 3.7. The simulations were performed in a constant temperature and constant volume ensemble (NVT) with three-dimensional periodic boundary conditions and coupled to Nosé-Hoover thermostat with relaxation times of 0.1 ps. Due to the large scale of generated cell, parameters were adapted for computational time consumption aspect. Shifted coulombic potential was used to calculate long range electrostatic interaction. All bonds were constrained using the SHAKE algorithm. The time step was 0.0025 ps and the interaction potential cutoff radius, which limits calculation of the interaction between molecules, was 14 angstrom.

The crystal slabs were first equilibrated for 500 ps at 4 different temperatures, 280, 300, 320, and 340 K. Then, 1500 α-resorcinol molecules were inserted randomly into the vacuum on both sides of the equilibrated crystal slabs. After equilibration, the crystal slab thickness was approximately 60 angstrom, whilst the vapour was approximately 50 angstrom.

The simulations were performed in a constant temperature and constant volume ensemble (NVT) with three-dimensional periodic boundary conditions and coupled to Nosé-Hoover thermostat with relaxation times of 0.1 ps. All simulations were continued at 280, 300, and 320 for 10 ns, except for the simulation at 340 K which was carried out for 5 ns as shown in Figure 3.8.

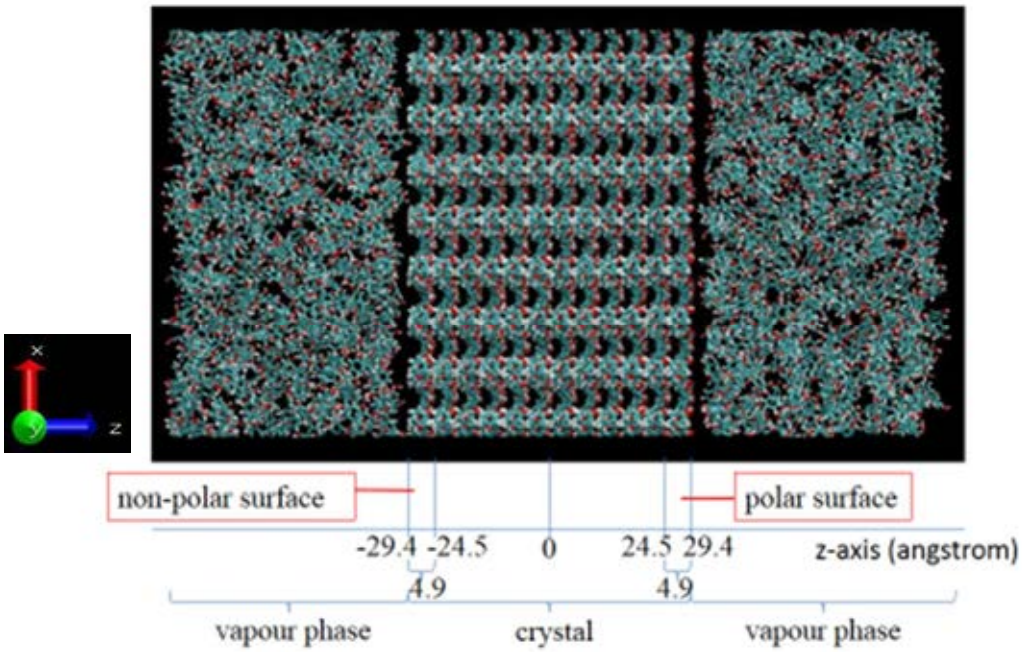

Figure 3.7 The 280 equilibrated structure of α-resorcinol crystal and vapour α-resorcinol used as starting configuration for simulating crystal growth from solution. The non-polar face, (011), is on the left and the polar face, $(0\bar{1}\bar{1})$, is on the right.

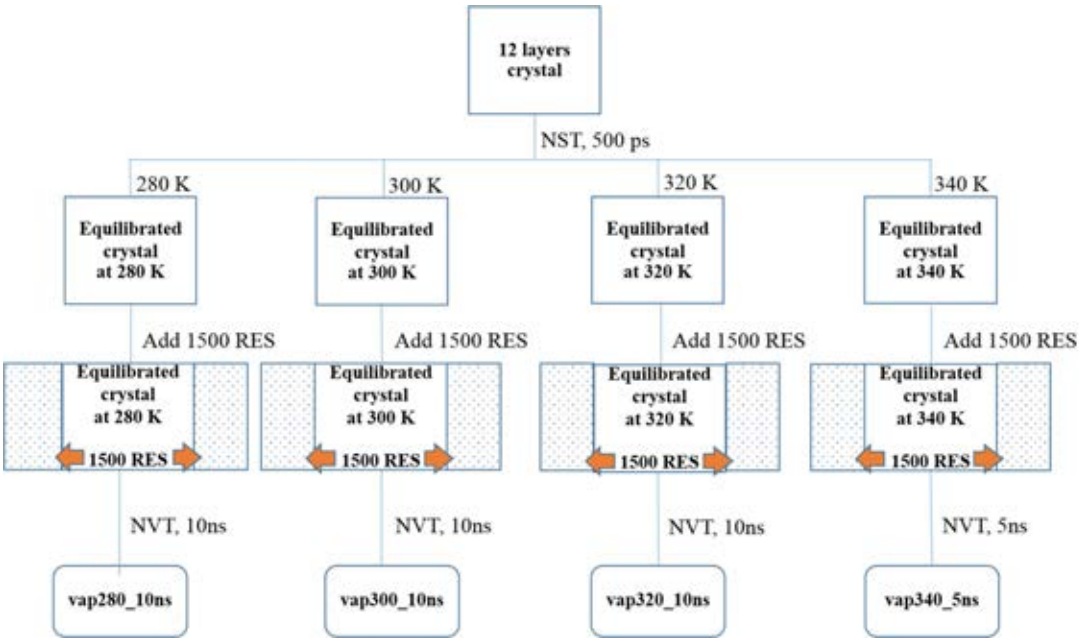

Figure 3.8 Schematic diagram showing the simulations of crystal growth from vapour. RES represents α-resorcinol molecule in vapour.

3.3.4 Crystal growth from the melt

A simulation cell was generated by in-house programs (J.Anwar, University of Bradford). It consisted of a crystal slab of α-resorcinol containing 3072 molecules with the non-polar face, (011), and the polar face, $(0\bar{1}\bar{1})$, exposed to 2500 melted α-resorcinol molecules which were generated to pack them on both faces denser than the vapour simulations as shown in Figure 3.9. The simulations were performed in a constant temperature and constant stress ensemble (NST) with three-dimensional periodic boundary conditions and coupled to Nosé-Hoover thermostat and barostat with relaxation times of 0.1 and 1.0 ps, respectively, were used to control temperature and pressure at 1 atm. Shifted coulombic potential was used to calculate long range electrostatic interaction. All bonds were constrained using the SHAKE algorithm. The

time step was 0.0025 ps and the interaction potential cutoff radius, which limits calculation of the interaction between molecules, was 14 angstrom.

The cells were initially generated with 3 different lengths along the z-axis: 200, 205, and 210 angstrom. Each cell was equilibrated for 800 ps at 300 K, with an increased mass for the resorcinol molecules (100 fold higher) in the force field input. The increased mass maintained the integrity of the crystals while allowing the melted α-resorcinol molecules to equilibrate about the exposed crystal faces. The choice of differing z-axis lengths was employed to generate different starting positions of the α-resorcinol molecules. After equilibration, the crystal slab thickness was approximately 60 angstrom, whilst the melted α-resorcinol layer was approximately 50 angstrom. (Figure 3.10).

The simulations using the 200 angstrom z-axis equilibrated configuration were carried out at 280, 300, and 320 K. A total of three replicate simulations using 200, 205, and 210 z-axis equilibrated configurations were carried at 300 K to remove any bias resulting from the starting configuration. All simulations were carried out for 30 ns as shown in Figure 3.11.

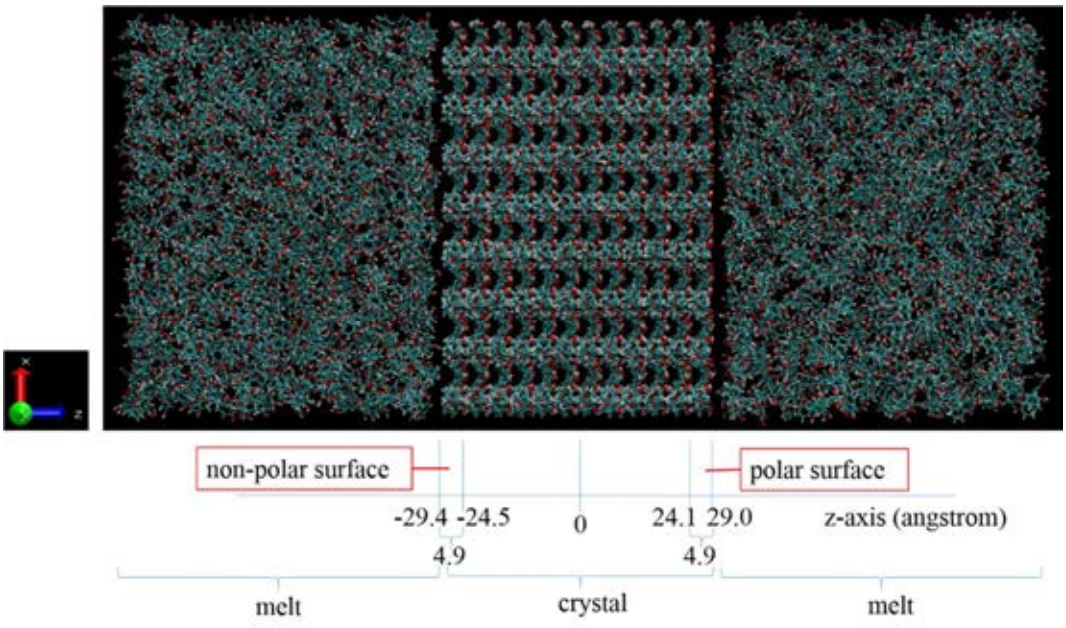

Figure 3.9 The structure of α-resorcinol crystal and melted α-resorcinol used as starting configuration. The non-polar face, (011), is on the left and the polar face, $(0\bar{1}\bar{1})$, is on the right. The z-axis cell dimension of this system is 200 angstrom.

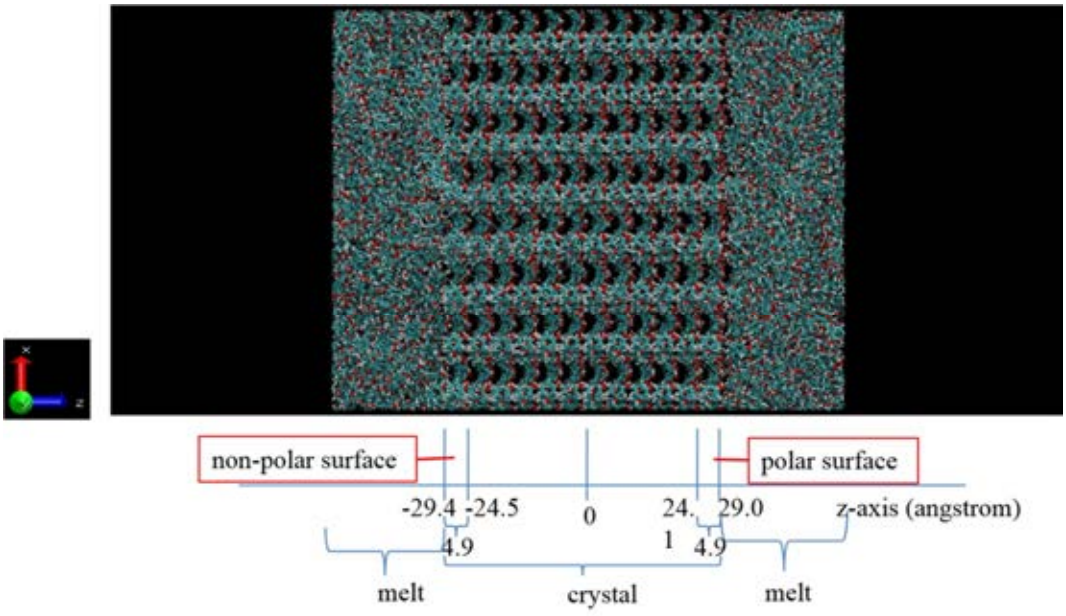

Figure 3.10 The 300 K equilibrated structure of α-resorcinol crystal and melted α-resorcinol used as starting configuration for simulating crystal growth from melt. The non-polar face, (011), is on the left and the polar face, $(0\bar{1}\bar{1})$, is on the right. The z-axis cell dimension of this system is 200 angstrom.

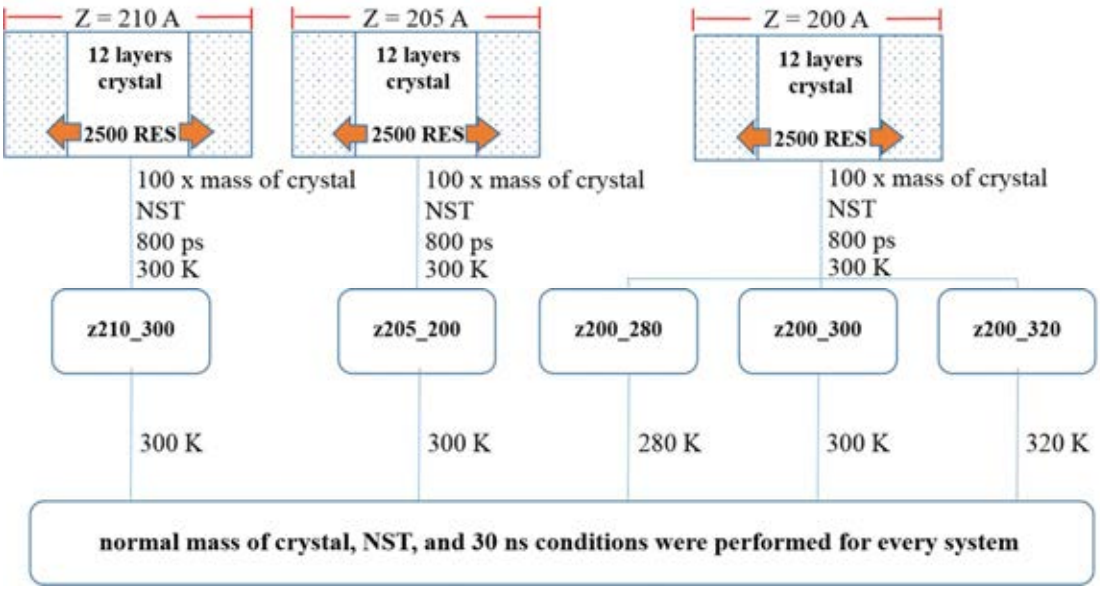

Figure 3.11 Schematic diagram showing the simulations of crystal growth from melt. RES represents melted α-resorcinol molecule.

3.4 Analysing the simulations

Molecular trajectories from all simulations were visualized by the program Visual Molecular Dynamics (VMD) (Humphrey et al., 1996) and determined by an in-house suite of analytical programs for density profiles and trajectory projections.

3.4.1 Density profiles

The variations in density of molecular species across the system were demonstrated in density profiles. The density profiles are excellent at identifying regions whether the molecules in a particular exist in the crystalline phase or not, and hence for following crystal growth or dissolution. The cell was divided into segments or layers corresponding to each layer of the crystal slabs which was 4.9 angstrom in

width along the z-axis. The centre-of-mass density of each molecular species in each segment was then calculated and plotted as a function of the z-dimension of the system.

3.4.2 Trajectory projections

The motions of molecular species in the system, especially near the crystal surface could be visualized by VMD program and shown by plotting the centre-of-mass trajectories of molecular species in a defined layer in the plane of the crystal surface (x-y plane). These layers could be defined using the data from the density profiles. Furthermore, the centre-of-mass trajectories of molecular species plot can examine the rate of dissolution and growth by fraction of coverage plot as a function of time, according to the Equation 3.1 (Langmuir, 1917):

$$\theta = \frac{x}{x_0} \qquad (3.1)$$

where θ represents fraction of surface coverage, x is the amount of occupied sites, and x_0 is the total amount of available sites in a complete layer.

CHAPTER IV

RESULTS AND DISSCUSION

4.1 Force field evaluation

The water density profiles from the simulations were plotted comparing with the experimental data as a function of temperature (Kell, 1975). The results show that the simulated water densities at the varied temperatures were corresponded with the experimental data. As a result of 293-333 K densities, the simulation results agreed with the experimental profiles; this temperature range was then selected to continue the later MD simulations of dissolution and crystal growth from solution.

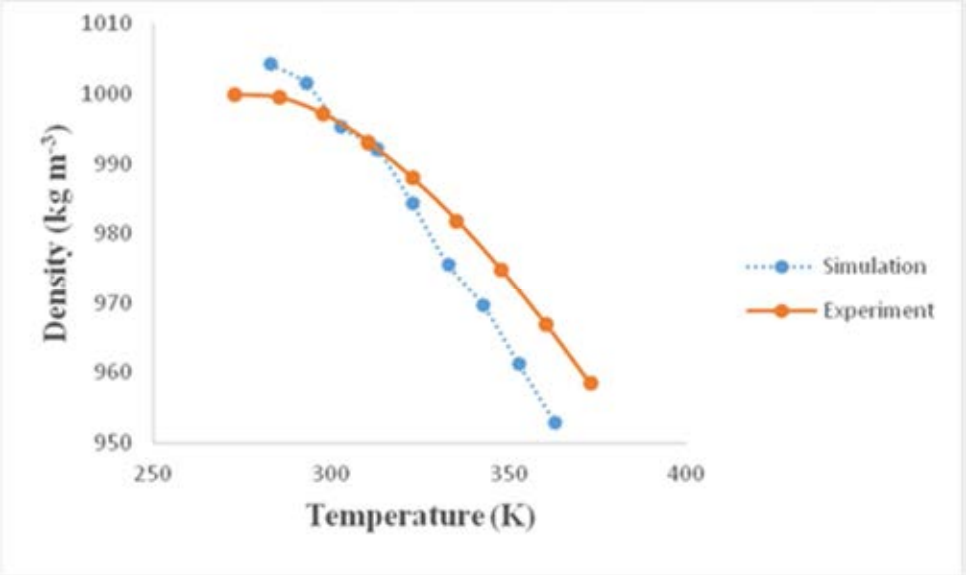

Figure 4.1 Water density profiles from simulations comparing with the experiment data.

4.2 Density profiles

4.2.1 Dissolution

The results of average densities over the first nanosecond of α-resorcinol crystal slab and water are shown in Figure 4.2. A water layer on the non-polar face was present at all temperatures studied, whilst the water layer on the polar face appeared only for simulation at 293 K.

After 15 ns, the crystal slab simulated at 333 K was completely dissolved into solution (Figure 4.3c), while the crystal slabs simulated at 293 K (Figure 4.3a) and 313 K (Figure 4.3b) were only partially dissolved. After simulation for a further 50 ns, at 293 K, only a single polar face layer had dissolved into solution while the non-polar face still retained its structure (Figure 4.4a). At 313 K, 3 layers of polar face and one layer of non-polar face had dissolved into solution after 50 ns (Figure 4.4b). This indicates that the temperature has a significant impact on the dissolution behavior of α-resorcinol. Formation of water layer occurred on the non-polar face because of dislike property between water molecule, which is polar, and non-polar crystal face, leading to inhibition of dissolution on non-polar face.

Repeat simulations at 333K using different starting configurations performed similarly as described above but with faster dissolution rates than the simulations at 293 and 313 K.

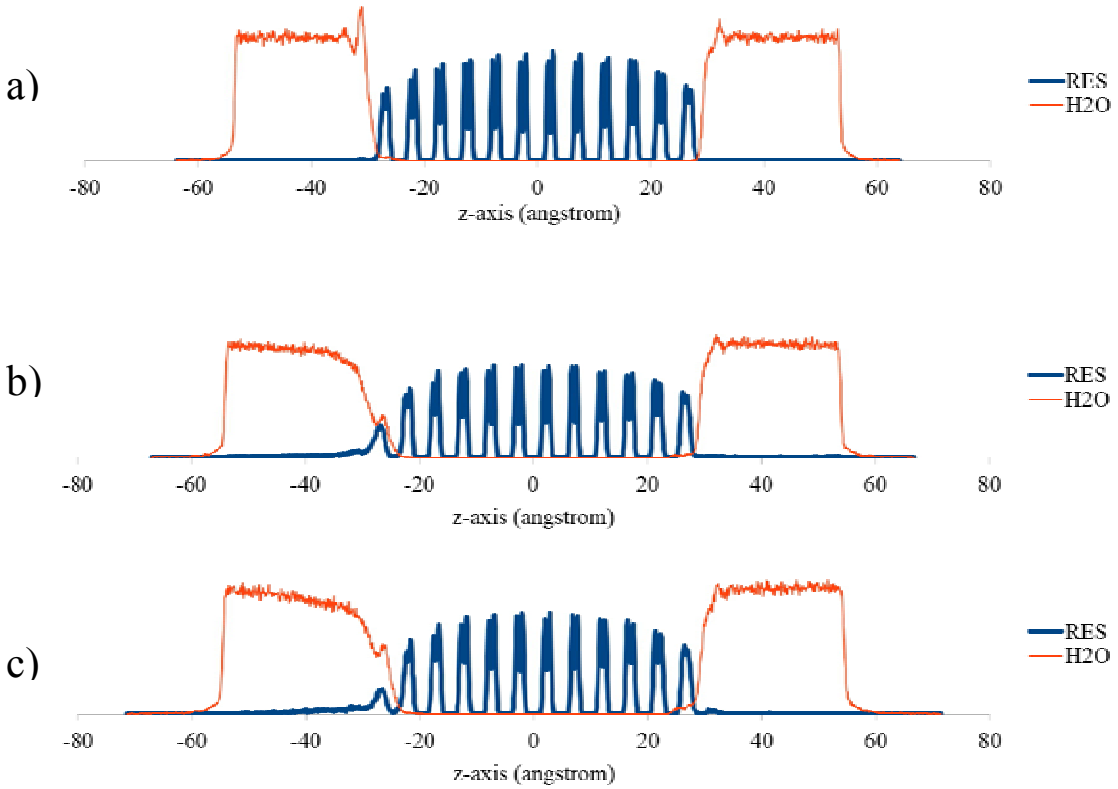

Figure 4.2 Average density profiles of α-resorcinol (RES) and water (H2O) along z axis over the first nanosecond of the dissolution simulations carried out at a) 293K, b) 313 K and c) 333 K with the 200 K starting configuration. The non-polar face, (011), is on the right and the polar face, $(0\bar{1}\bar{1})$, is on the left.

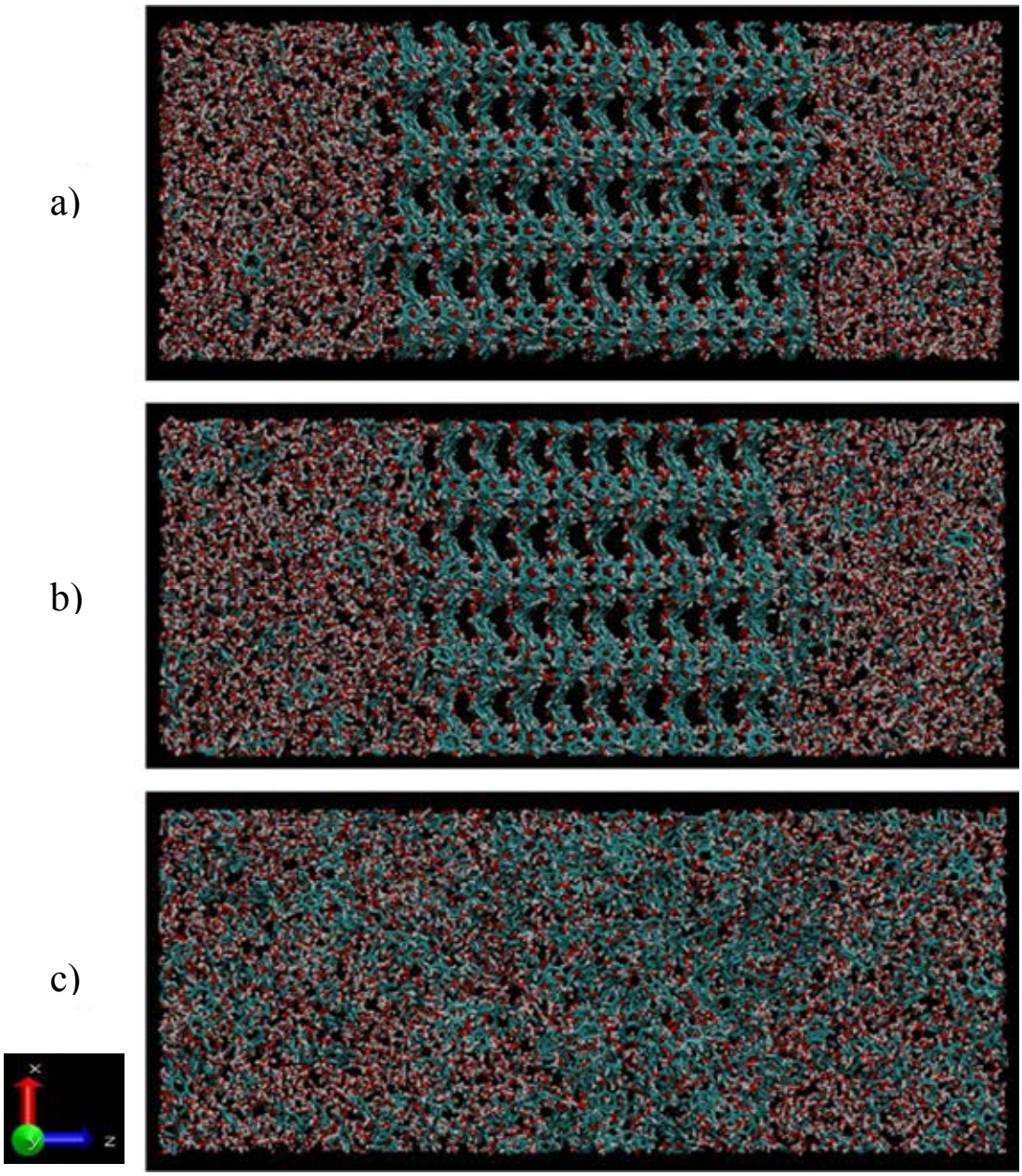

Figure 4.3 Snapshots of dissolution after 15 ns; the non-polar face, (011) is on the right, and the polar face, $(0\bar{1}\bar{1})$ is on the left. The temperatures of the dissolution simulation are; a) 293 K, b) 313 K and c) 333 K and the starting configuration was taken from a simulation at 200 K.

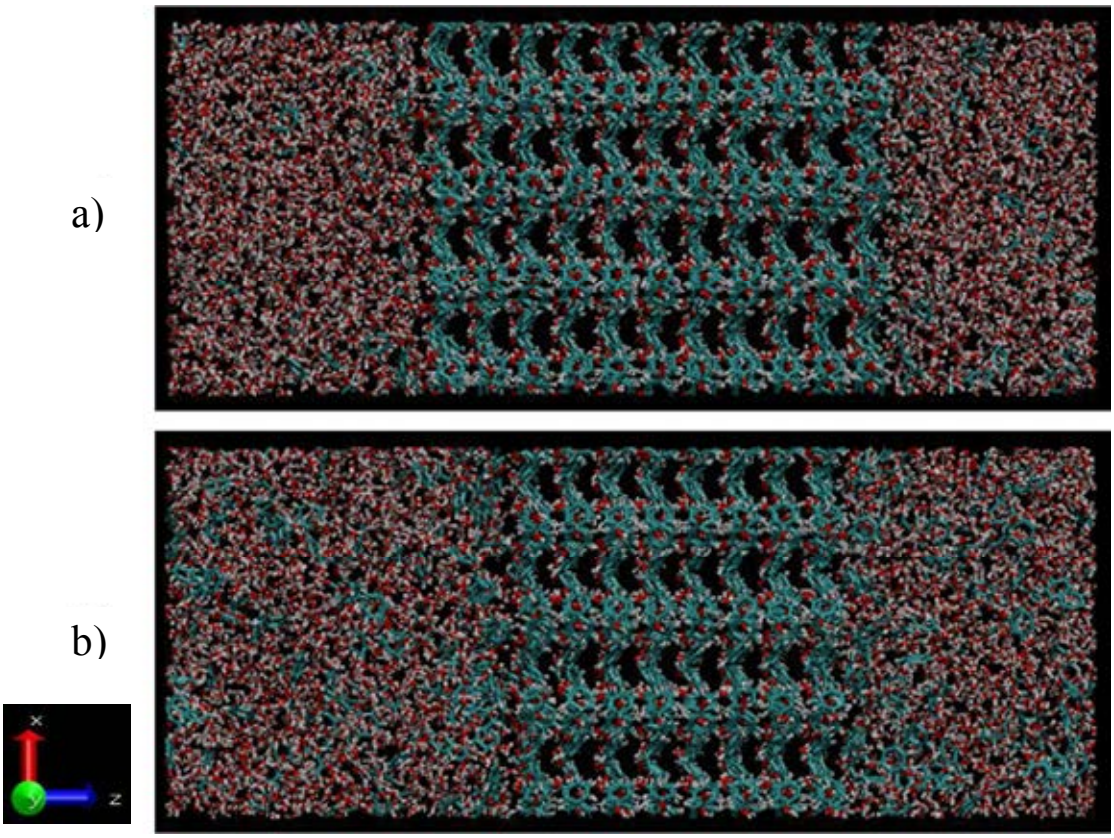

Figure 4.4 Snapshots of the dissolution simulations after 65 ns. The non-polar face, (011), is on the right, and the polar face, ($0\bar{1}\bar{1}$), is on the left. The temperatures of the simulations are a) 293 K, b) 313 K.

4.2.2 Crystal growth from solution

The results of average densities over the first nanosecond of water and α-resorcinol at 293 K are shown in Figure 4.5. In all simulations, a higher density of resorcinol was found on the polar face compared with the non-polar face. Similar results were observed in previous studies (Davey et al., 1988; Srinivasan and Sherwood, 2005). The densities of resorcinol molecules on polar faces in the simulations with different ratios of resorcinol to water molecules were similar, while the variation in the densities of water molecules was found on non-polar faces. The higher the supersaturation, the denser were resorcinol molecules on the non-polar face. However, the growth rate on

non-polar face was not different. This may be explained by self-poisoning mechanism which inhibits crystal growth on (011) face (Weissbuch, 2006).

After 65 ns, the simulation with the lowest level of supersaturation showed three and one growth layers on the polar and non-polar faces, respectively (Figure 4.6a). The simulation with the medium level of supersaturation appeared to gain five growth layers on polar face, while no growth layer was observed on non-polar face (Figure 4.6b).

For replicated simulations of different starting configurations with the highest level of supersaturation, there were four growth layers on polar face in the simulation using the starting configuration prepared at 200 K and five growth layers for other starting configurations (Figure 4.6c). However, in all replicates, there was only one growth layer on the non-polar face.

The results indicate that higher level of supersaturation induce crystal growth, in particular on the polar face. A polar face shows higher growth rates as attachment to the surface is more favorable for free resorcinol molecules in the solution as they have a higher concentration. On a non-polar face, the formation of growth layers was slower because of the reduced number of free resorcinol molecules. Due to a little different number of growth layers on polar faces of replicate simulations, the starting configuration might affect the crystal growth process.

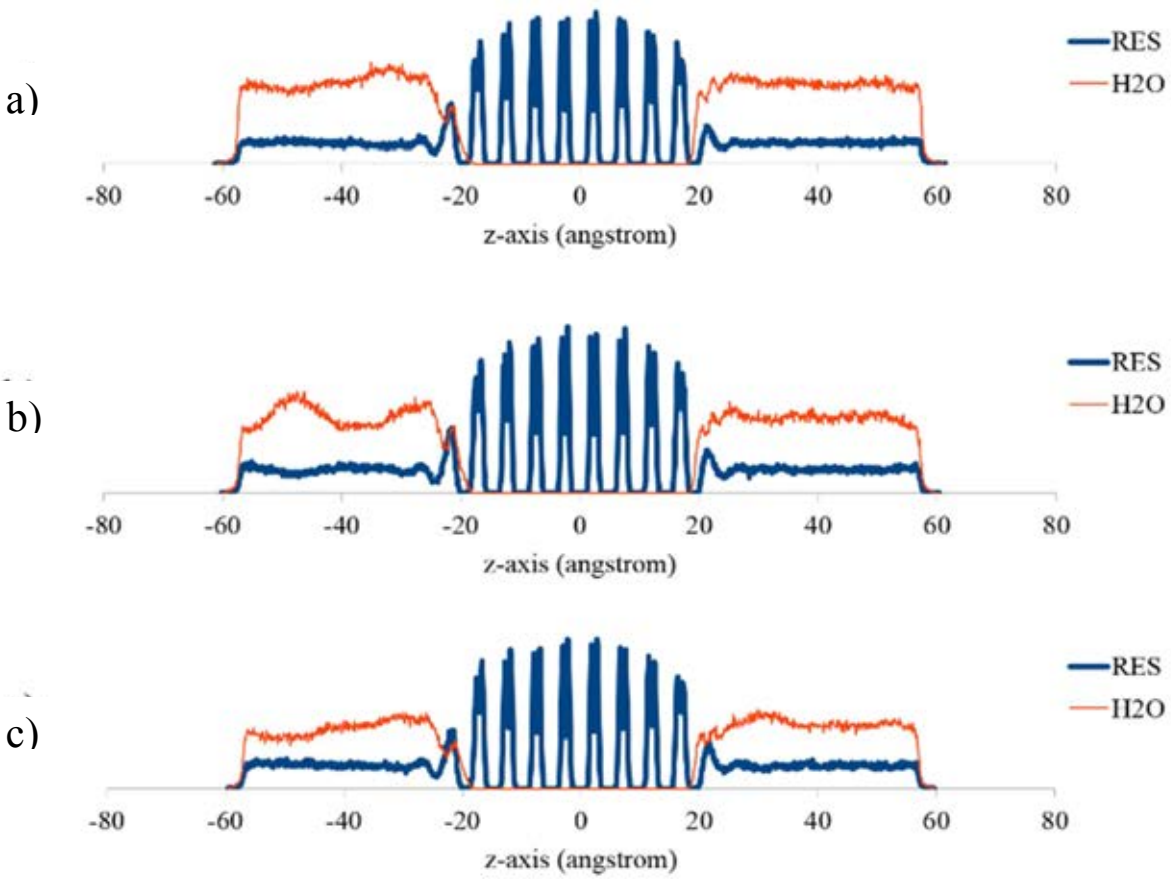

Figure 4.5 Average density profiles of α-resorcinol (RES) and water (H2O) along z axis after the first nanosecond of the crystal growth from solution simulations at 293 K using the 200K starting configurations comprising different ratios of resorcinol : water (RES:H2O); a) 549:2122, b) 593:1850, and c) 631:1621. The non-polar face, (011), is on the right and the polar face, $(0\bar{1}\bar{1})$, is on the left.

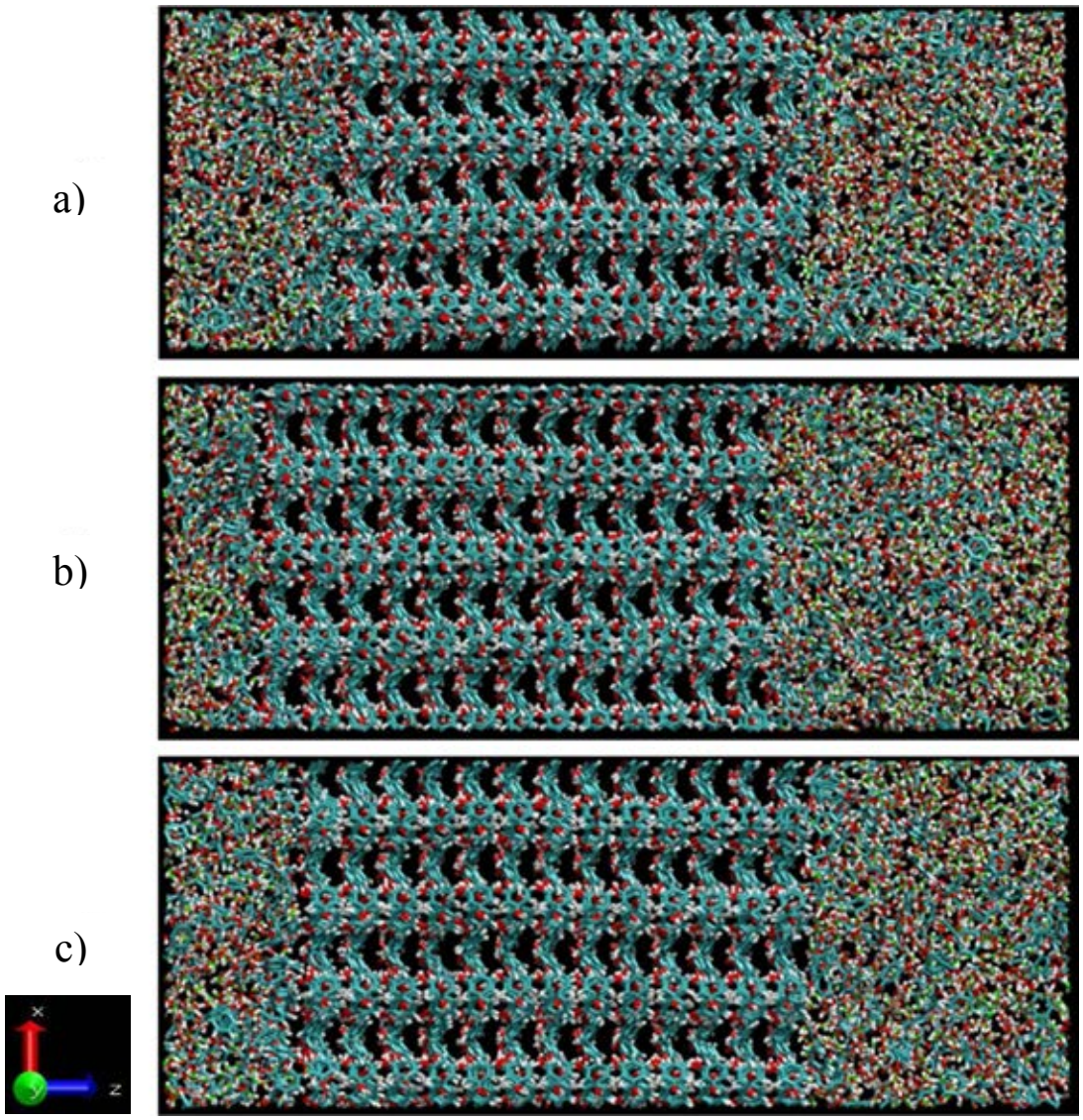

Figure 4.6 Snapshots at 65 ns of the crystal growth from solution simulations at 293K using the 200 K starting configuration, showing the non-polar face, (011), on the right, and the polar face, $(0\bar{1}\bar{1})$, on the left. The ratios of α-resorcinol to water (RES:H2O) are; a) 549:2122, b) 593:1850, and c) 631:1621.

4.2.3 Crystal growth from vapour

Both faces of resorcinol crystal slab simulated at 340 K had clearly sublimed at 5 ns as shown in Figure 4.7. Therefore, the simulation at this temperature was not continued. Simulations at all other temperatures were performed for a period of 5 ns.

The results of average densities over the last nanosecond for all simulations at the end of 10 ns are shown in Figure 4.8. Growth layers on both faces were seen in all simulations at 280, 300, and 320 K. At 280 K, there were two growth layers on the polar face and one growth layer on the non-polar face (Figure 4.9a). In contrast, the one growth layer on the polar face and two growth layers on the non-polar face appeared in the 300 K simulation (Figure 4.9b). At 320 K, both faces lost some resorcinol molecules into vapour phase, mainly from the polar face. However, the vacancies on both faces were filled by free resorcinol molecules from the vapour phase and one growth layer was seen on the non-polar face (Figure 4.9c). This can be explained by the fact that the high temperature of 300 and 320 K induced sublimation at the crystal faces, causing disarrangement of the resorcinol molecules on the surface. The sublimation was more progressive on the polar face that were agree with self poisoning mechanism study (Weissbuch, 2006), while the disorder of surfaces were different from the previous simulations of the crystal slab in vacuum (Anwar et al, 2007). The unstructured polar face would delay the arrangement of vapour molecule on the crystal surface as shown in Figure 4.10.

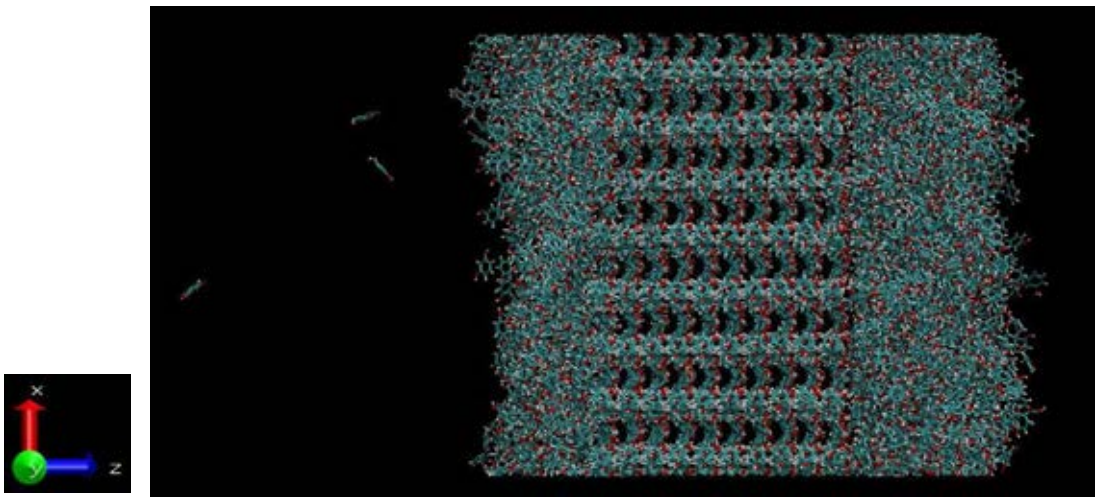

Figure 4.7 Snapshots of crystal growth from vapour simulations the non-polar face, (011), on the left, and the polar face, $(0\bar{1}\bar{1})$, on the right simulated at 5 ns of 340 K simulation.

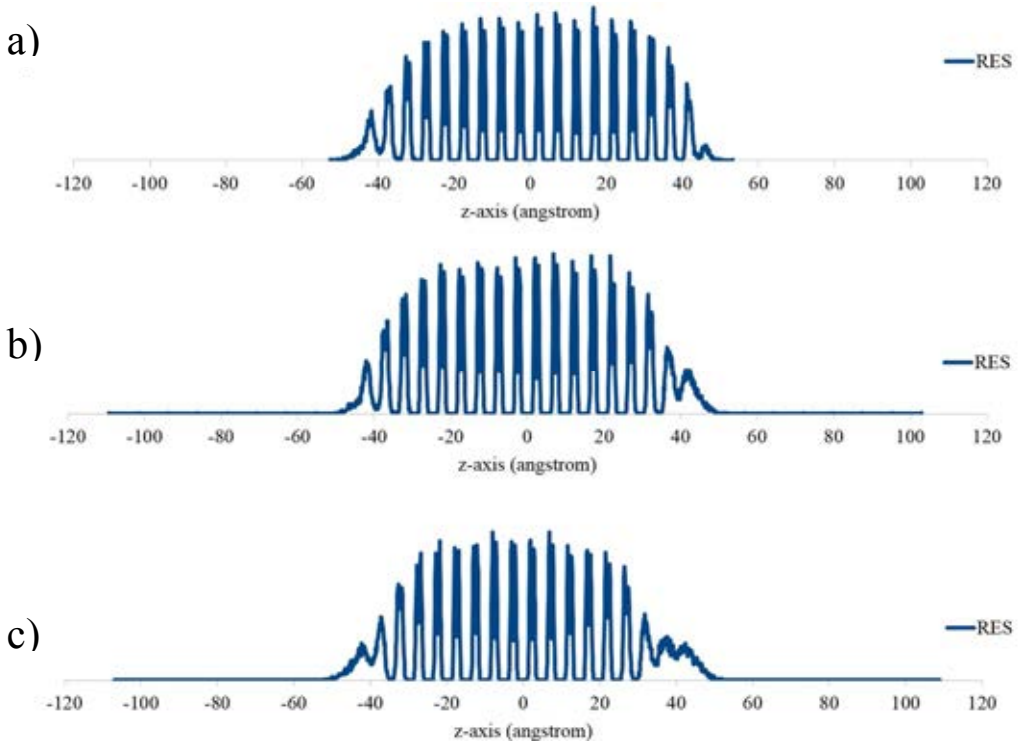

Figure 4.8 Average density profiles of α-resorcinol (RES) along z axis over the last nanosecond of 10 ns crystal growth from vapour simulations using the 200 K starting configuration. The temperatures of the simulations were; a) 280 K, b) 300 K, and c) 320 K. The non-polar face, (011), is on the left and the polar face, $(0\bar{1}\bar{1})$, is on the right.

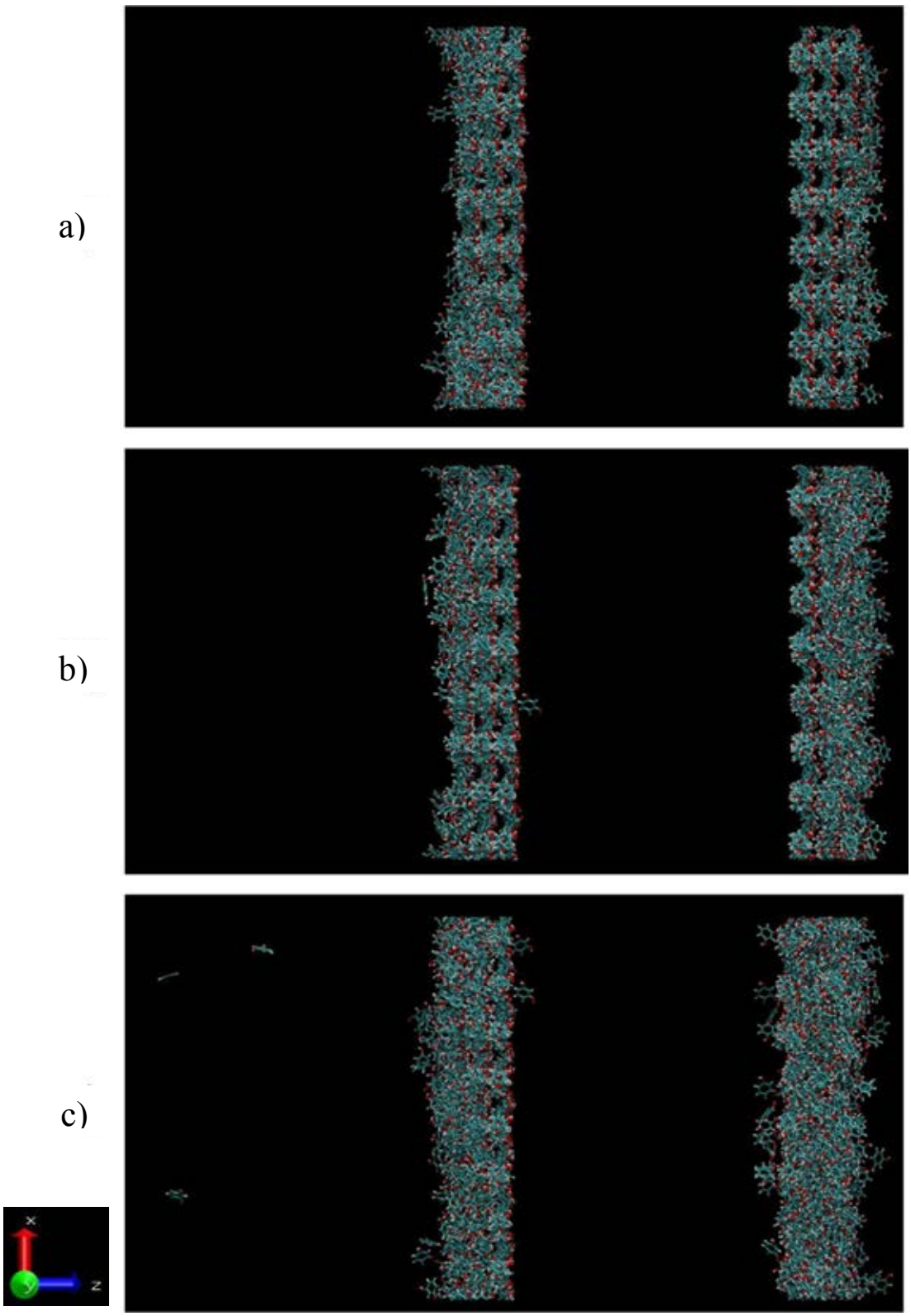

Figure 4.9 Snapshots of α-resorcinol in the vapour phase at 10 ns in which some molecules attach and form growth layers on both polar face, $(0\bar{1}\bar{1})$, and non-polar face,(011), on the right and left, respectively, at different temperatures; a) 280 K, b) 300 K, and c) 320 K. These simulations used the 200 K starting configuration.

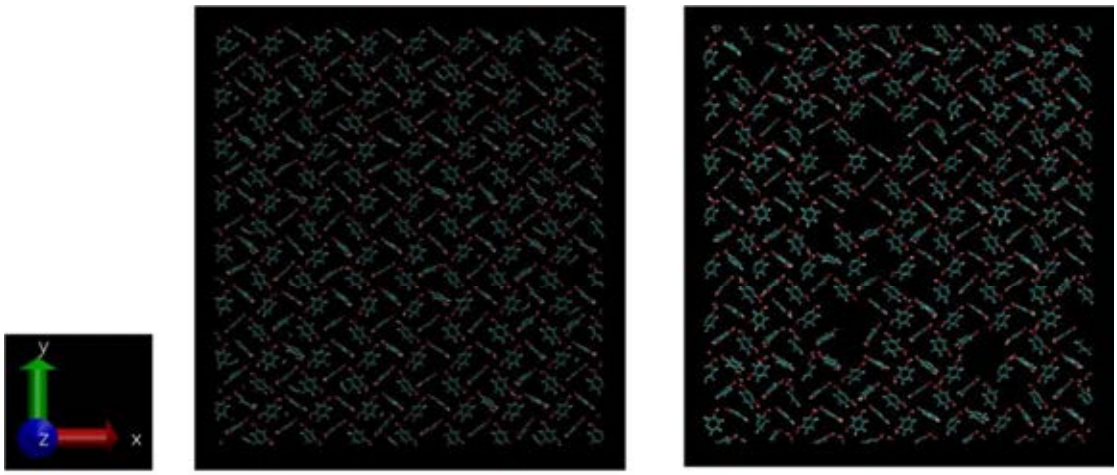

Figure 4.10 The surface orientation at 10 ns of a) non-polar face, (011), and b) polar face, $(0\bar{1}\bar{1})$, of crystal growth from vapour at 320 K.

4.2.4 Crystal growth from melt

The results of average densities over the last nanosecond of the 30 ns runs are shown in Figure 4.11. Growth layers on both faces were observed in all simulations at 280, 300, and 320 K were observed. There were two growth layers on the polar face and one layer on the non-polar face appearing in the simulations at 280 K (Figure 4.12a) and 320 K (Figure 4.12c). For the replicated simulations with different starting z-axis lengths, carried out at 300 K, there were three growth layers on the polar face and one growth layer on the non-polar face. In Figure 4.12b, a snapshot of the simulation using the 200 angstrom starting configuration is shown.

There may be an optimum temperature for crystal growth from melts. At high temperatures, the resorcinol molecules possessed high kinetic energy leading to more mobility. Compared with crystal growth at 280 K, more growth layers are obtained at 300 K because the resorcinol molecules from melt are more mobile. However, at 320

K, it is possible that the crystal surface is disordered, so that it is more difficult for free resorcinol molecules to form new layers.

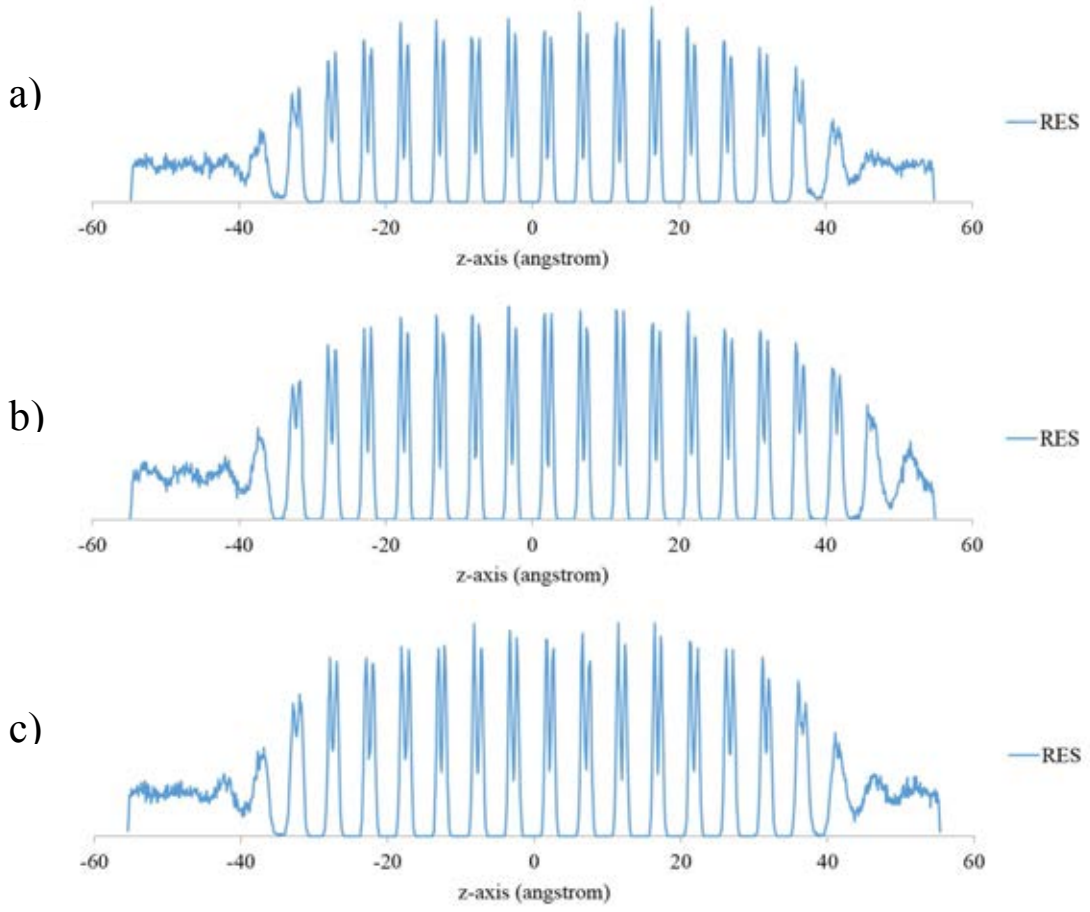

Figure 4.11 Average density profiles of α-resorcinol (RES) along z axis over the last nanosecond of 30 ns crystal growth from melt simulations using the 200 angstrom z-axis length starting configuration. The temperatures of the simulations were; a) 280 K, b) 300 K, and c) 320 K. The non-polar face, (011), is on the left and the polar face, $(0\bar{1}\bar{1})$, is on the right.

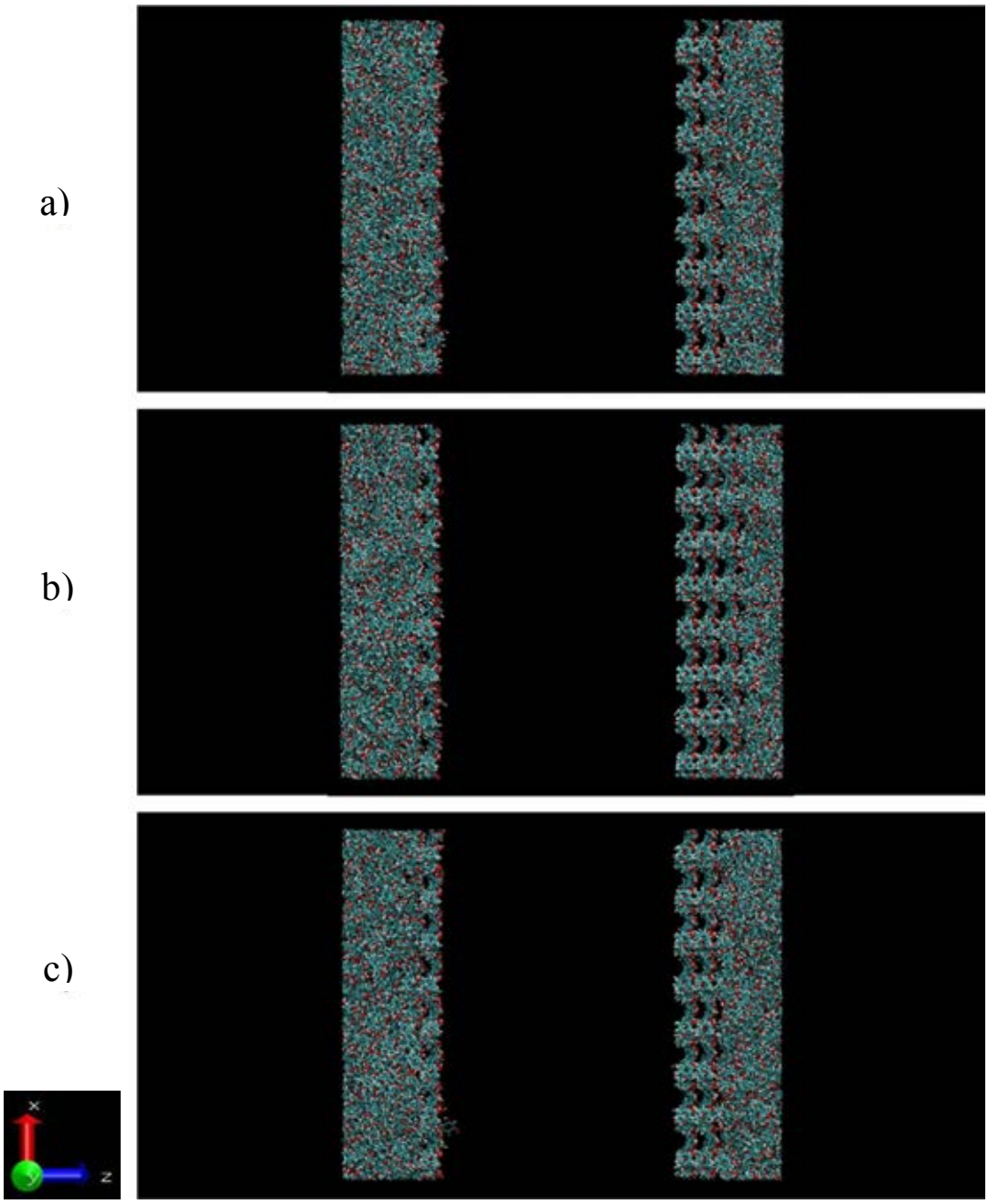

Figure 4.12 Snapshots at 30ns of melted α-resorcinol using the 200 angstrom z-axis length starting configuration, in which some molecules attach and form growth layers on both polar face, $(0\bar{1}\bar{1})$, and non-polar,(011), on the right and left, respectively. The temperatures of the simulations are; a) 280 K, b) 300 K, and c) 320 K.

4.3 Trajectory projections

4.3.1 Dissolution

Trajectory profiles (Figure 4.13) show that resorcinol molecules dissolve into the solvent medium after a period of simulation. Initially, the crystal slab is intact. The dissolution of crystal is dependent on the temperature. Clearly, at higher temperature, more crystal dissolves. In addition, at 333 K, none of the crystal could retain any of its structure after 15 ns. The trajectories also show differences in dissolution rate for each face (Figure 4.13). At the same temperatures of 293, 313, and 333 K, the polar face dissolves faster than the non-polar face. The fraction of surface coverage was calculated based on the number of resorcinol molecules within the defined range of 4.9 angstrom, representing one crystal layer. This value was employed to estimate the density of the resorcinol molecules either in the crystal slab or in the surrounding solvent. When the estimation was made with respect to the crystal slab, the reduced number of fraction of surface coverage implies that there are some molecules which have dissolved into the bulk medium. When the estimation is made with respect to the solvent, the increased number of fraction of surface coverage indicates that there are some molecules which have migrated to the solvent. After 65 ns, at 293 (Figure 4.13a, 4.13d) and 313 K (Figure 4.13b, 4.13e), it was observed that the values of fraction of surface coverage of crystal slab and bulk medium were constant. This may be due to saturated state of solutions at these temperatures.

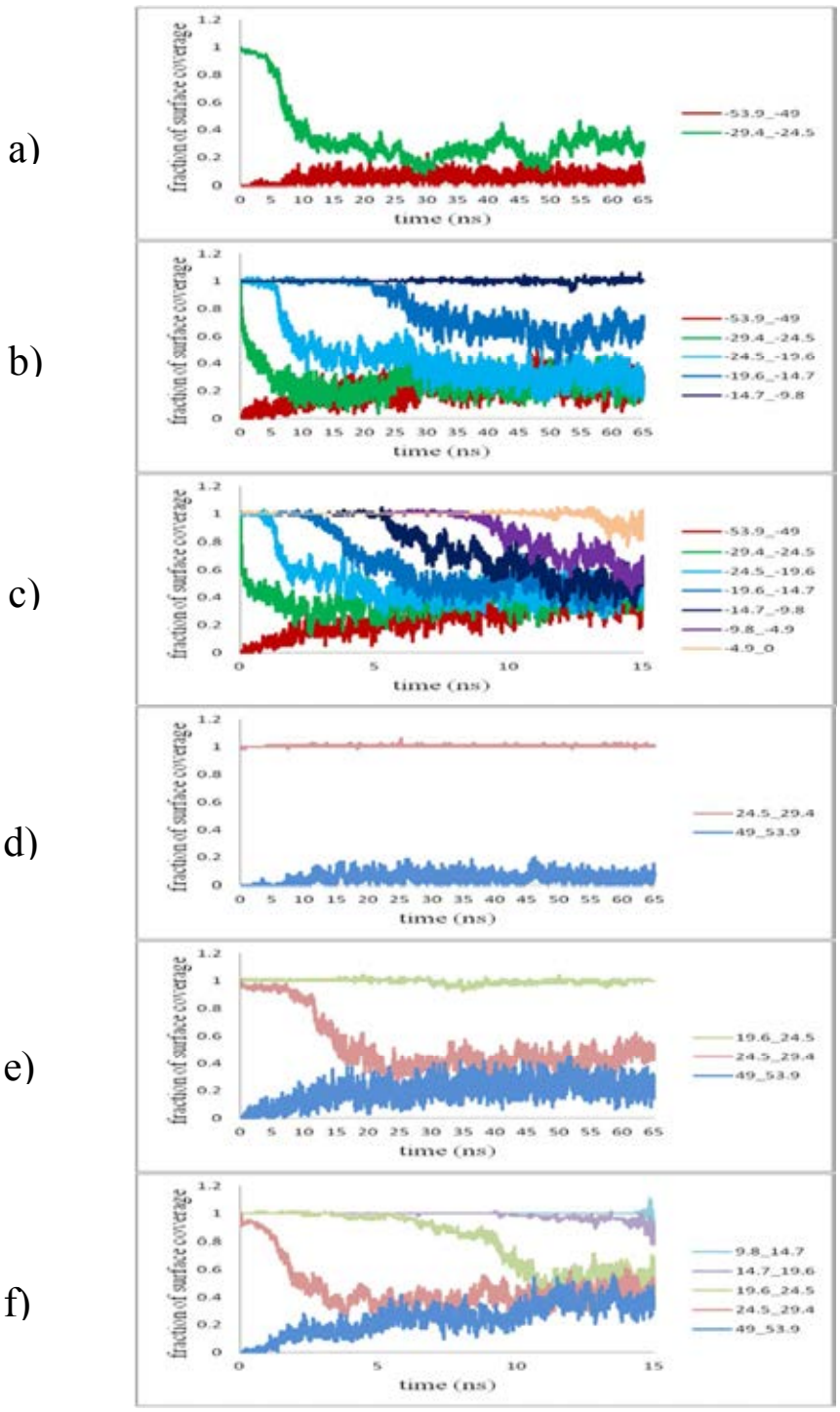

Figure 4.13 Fraction of surface coverage as a function of time on the polar face, $(0\bar{1}\bar{1})$, and the non-polar face, (011), for the dissolution simulations at 293 K (a, d), 313 K (b, e), and 333 K (c, f) with starting configurations at 200 K. Numbers of each label represent the range (angstrom) from the center of the system.

4.3.2 Crystal growth from solution

Trajectory profiles (Figure 4.14) show that there are resorcinol molecules attached to the crystal faces. The reduced values of fractional surface coverage, estimated on the basis of the solvent region, confirm that the solute molecules of resorcinol form additional layers on both crystal faces. According to the fractional surface coverage from all simulations, the growth process of the following layer proceeds while the former growing layer is still incomplete (Figure 4.14).

According to the simulations, crystal growth occurs on the polar face faster than on the non-polar face. Also, the results agree with the experimental data (Davey et al., 1988) that the level of supersaturation affects the crystal growth process. The optimum level of supersaturation found in the present study was the middle level (S = 1.3). This might be explained that normally higher α-resorcinol molecules in solution increased the probability of molecules to attach and form a layer at the crystal surface. However, extensively higher number of molecules might compete each in the attachment to the crystal surface in forming a uniform layer.

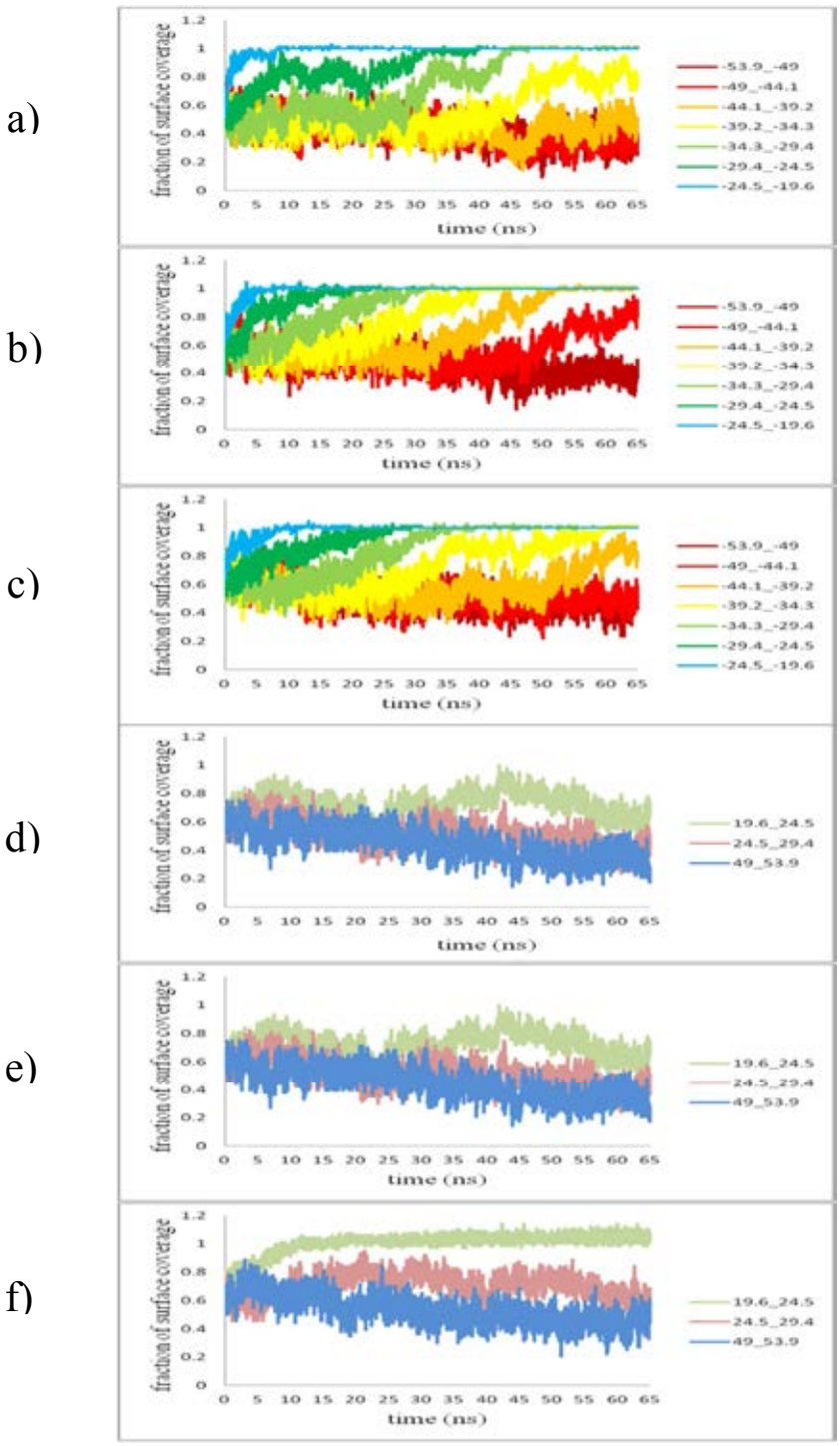

Figure 4.14 Fraction of surface coverage as a function of time of the polar face, $(0\bar{1}\bar{1})$, and the non-polar face, (011), for different ratios of resorcinol: water (RES: H2O) of the crystal growth from solution simulations; a, d) 549:2122, b, e) 593:1850, and c, f) 631:1621 with starting configurations at 200 K. Numbers of each label represent the range (angstrom) from the center of system.

4.3.3 Crystal growth from vapour

Trajectory profiles (Figure 4.15) show that α-resorcinol molecules from the vapour move onto and attach to both crystal faces. The first growth layer of the polar face forms faster than that of the non-polar face (Figure 4.16).

At the beginning of all simulations, the fraction of surface coverage in the range for the first growth layer on the polar face immediately increased to 1, implying one full growth layer as shown in Figure 4.16. The molecules in the vapour phase may prefer the polar to the non-polar face because of attraction between the hydroxyl groups of free α-resorcinol molecules and polar face. At 320 K, fluctuations in the values of the fraction of surface coverage around 1.0 over the simulation were observed for the polar surface. This is due to a higher number of resorcinol molecules within the relevant range of the polar face.

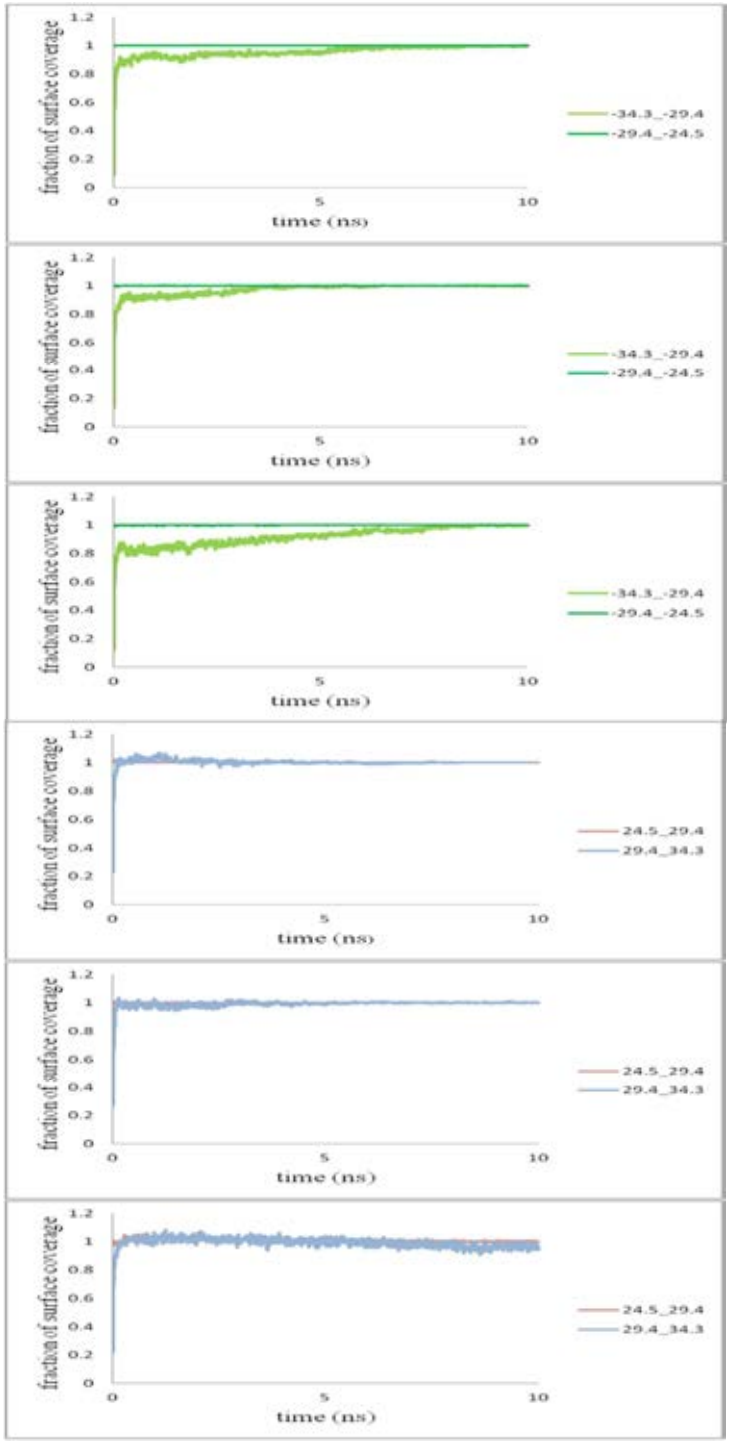

Figure 4.15 Fraction of surface coverage as a function of time of the non-polar face, (011), and the polar face, $(0\bar{1}\bar{1})$, for the crystal growth from vapour simulations at 280 K (a, d), 300 K (b, e), and 320 K (c, f) with starting configurations at 200 K. Numbers of each label represent the range (angstrom) from the center of system.

a)

b)

c)

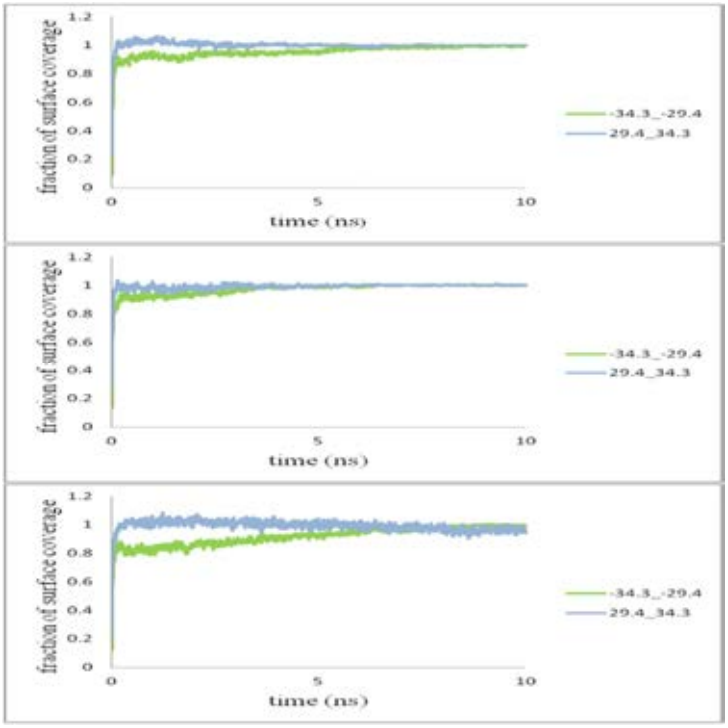

Figure 4.16 Fraction of surface coverage as a function of time on the polar face, $(0\bar{1}\bar{1})$, and the non-polar face, (011), of the crystal growth from vapour simulations for different temperatures; a) 280 K, b) 300 K, and c) 320 K with starting configurations at 200 K. Numbers of each label represent the range (angstrom) from the center of system.

4.3.4 Crystal growth from melt

Trajectory profiles (Figure 4.18) show α-resorcinol molecules from the melt appearing on both crystal faces. Crystal growth occurs on the polar face faster than on the non-polar face (Figure 4.18). On the polar face, there are more molecules from the melt attaching within the surfaces range at the beginning of then simulations (Figure 4.17d, 4.17e, and 4.17f). On the other hand, the non-polar face almost had no molecules from the melt attaching within the surface range. In the case of the first growth layers, a faster growth-rate was observed on the polar face when carried out at higher temperatures (Figure 4.17).

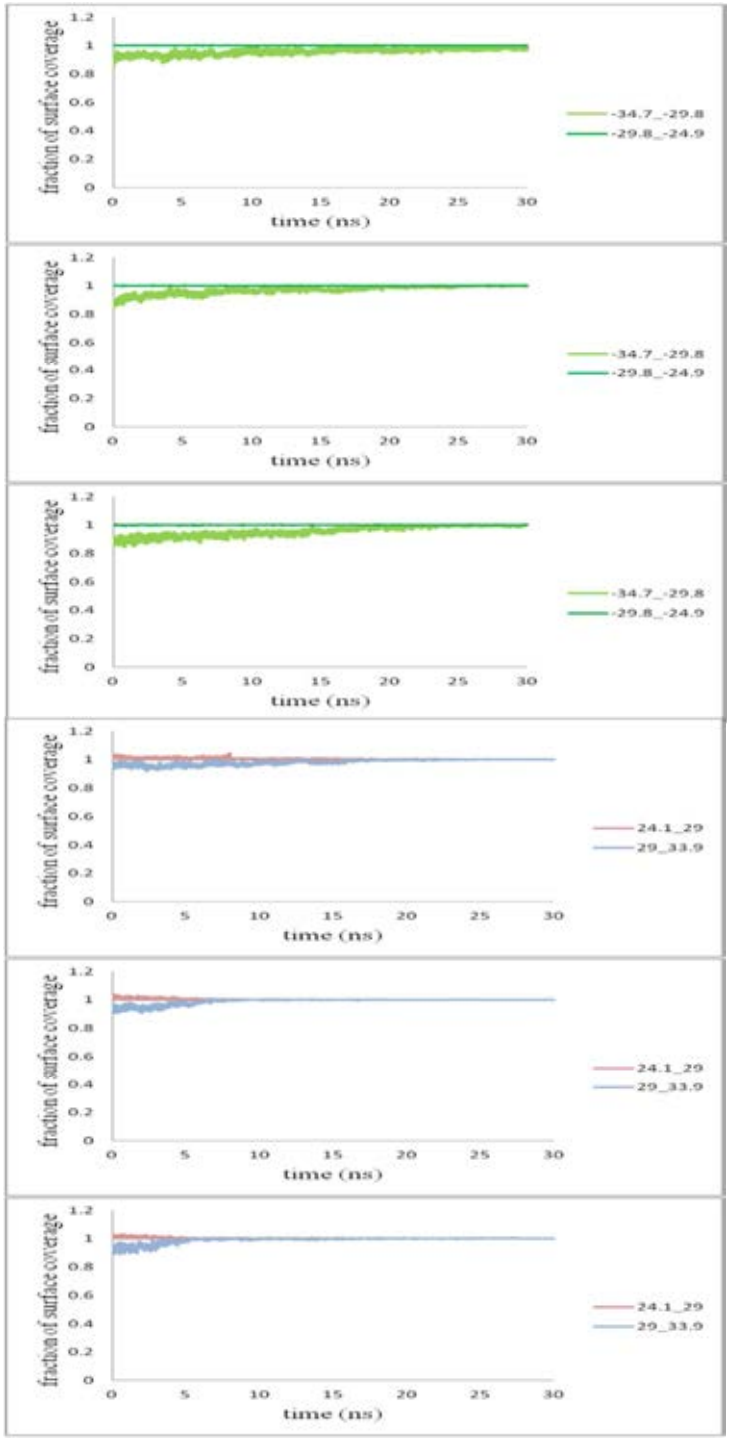

Figure 4.17 Fraction of surface coverage as a function of time on the polar face, $(0\bar{1}\bar{1})$, and the non-polar face, (011), for the crystal growth from melt simulations at a, d) 280 K, b, e) 300 K, and c, f) 320 K with 200 angstrom z-axis starting configurations. Numbers of each label represent the range (angstrom) from the center of system.

a)

b)

c)

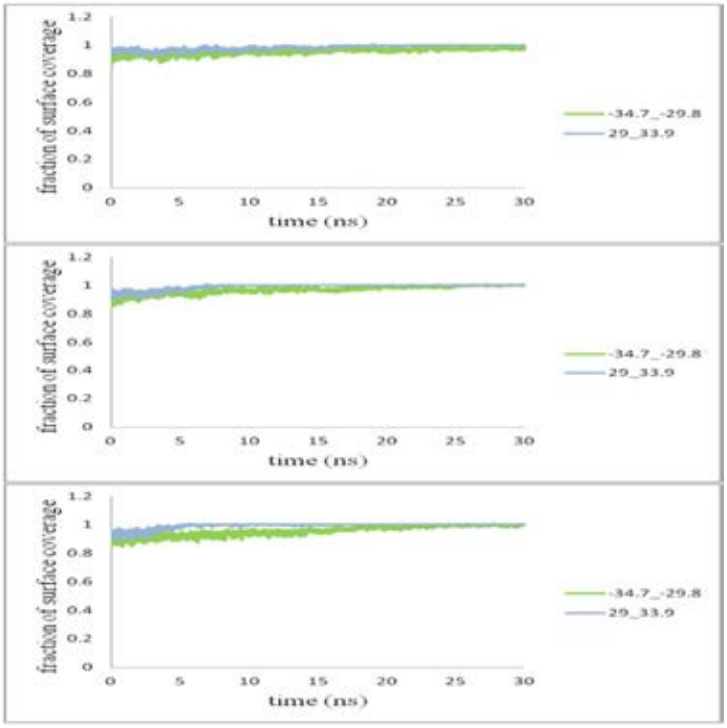

Figure 4.18 Fraction of surface coverage as a function of time of the polar face, $(0\bar{1}\bar{1})$, and the non-polar face, (011), of the crystal growth from melt simulations for different temperatures; a) 280 K, b) 300 K, and c) 320 K with 200 angstrom z-axis starting configurations. Numbers of each label represent the range (angstrom) from the center of system.

. CHAPTER V

CONCLUSION

Molecular dynamics simulations were performed to explore crystal growth and dissolution phenomena on (011) and $(0\bar{1}\bar{1})$ faces of α-resorcinol crystal. The results of crystal growth from supersaturated solution and from vapour simulations confirm the previous asymmetric growth of α-resorcinol crystal observed in experimental studies in which $(0\bar{1}\bar{1})$ faces was the faster growing. However, at the high temperature, in crystal growth from vapour simulation, the reconstruction appears especially on $(0\bar{1}\bar{1})$ face, which is in contrast to the previous surface reconstruction study.

The effect of solvent on crystal growth and dissolution of α-resorcinol was investigated. The water layer appearing on (011) face might cause inhibition of both dissolution and growth processes because of localization of the water layer on the surface. The water layer can be removed by increasing energy. Hence, the crystal can dissolve more at the higher temperatures. Additionally, rising number of free α-resorcinol molecules in the supersaturated solution enhanced the growth on $(0\bar{1}\bar{1})$ face, although more α-resorcinol molecules also appeared on (011) face. Possibly, the self-poisoning mechanism inhibits the growth process on (011) face.

Crystal growth from vapour and melt simulations were performed to remove the solvent effect and investigate an interaction between the crystal surface and free α-resorcinol molecules, also surface reconstruction. The density of free α-resorcinol molecules might be an important factor for interactions. Lower density of free α-resorcinol molecules in vapour phase might not have enough interaction to the crystal

surface, resulting in surface reconstruction which inhibits the growth on $(0\bar{1}\bar{1})$ face at the high temperature. The surface reconstruction might be hindered due to higher density of free α-resorcinol molecules on the crystal surface, as this is shown in crystal growth from melt.

The conclusion, however, needs confirmation by calculating surface-water adsorption energy, dipole moment, and surface-free molecules interaction energy. The surface-water adsorption energy may reveal more information about the dissolution. The dipole moment calculation may identify the direction of free α-resorcinol molecules in contact with crystal surfaces. The surface-free molecules energy would provide details about the interaction phenomena on surface, especially in crystal growth from vapour and melt simulations.

REFERENCES

Allen, M. P. and Tildesley, D. J. 1987. Computer simulation of liquids. Oxford: Oxford University Press.

Anwar, J., Jittima Chatchawalsaisin., and Kendrick, J. 2007. Asymmetric crystal growth of α-resorcinol from the vapor phase: Surface reconstruction and conformational change are the culprits. Angew Chem Int Edit 46(29): 5537-5540.

Berkovitch-Yellin, Z. 1985. Toward an ab initio derivation of crystal morphology. J Am Chem Soc 107(26): 8239-8253.

Bhat, M. N., and Dharmaprakash, S. M. 2002. Effect of solvents on the growth morphology and physical characteristics of nonlinear optical γ-glycine crystals. J Cryst Growth 242(1–2): 245-252.

Boek, E. S., Feil, D., Briels, W. J., and Bennema, P. 1991. From wave function to crystal morphology: application to urea and alpha-glycine. J Cryst Growth 114(3): 389-410.

Born, M. and von Kármán, T. 1912. Über schwingungen in Raumgittern. Phys Z 13: 279: 309.

Chatchawalsaisin, J., Kendrick, J., Tuble, S. C., and Anwar, J. 2008. An optimized force field for crystalline phases of resorcinol. Cryst Eng Comm 10(4): 437-445.

Cornell, W. D., et al. 1995. A 2nd generation force-field for the simulation of proteins, nucleic-acids, and organic-molecules. J Am Chem Soc 117: 5179-5197.

Davey, R. J., Milisavljevic, B., and Bourne, J. R. 1988. Solvent interactions at crystal surfaces: the kinetic story of .alpha.-resorcinol. J Phys Chem 92(7): 2032-2036.

de Leeuw, N. H., Harding, J. H., and Parker, S. C. 2002. Molecular dynamics simulations of the incorporation of Mg2+, Cd2+ and Sr2+ at calcite growth steps: introduction of a SrCO3 potential model. Mol Simulat 28(6): 573-589.

Essmann, U., Perera, L., Berkowitz, M. L., Darden, T., Lee, S., and Pedersen, L. G. 1995. A smooth particle mesh Ewald method. J Chem Phys 103(19): 8577-8593.

Ewald, P. P. 1921. Die Berechnung optischer und elektrostatischer Gitterpotentiale. Annalen der Physik 369(3): 253-287.

Hahn, S., Kielhorn, J., Koppenhöfer, J., Wibbertmann, A., and Mangelsdorf, I. 2006. Concise international chemical assessment document 71: Resorcinol. Hanover: WHO.

Hartman, P., and Bennema, P. 1980. The attachment energy as a habit controlling factor: I. Theoretical considerations. J Cryst Growth 49(1): 145-156.

Hernandes, M. Z., Da Silva, J. B. P., and Longo, R. L. 2003. Chemometric study of liquid water simulations. I. The parameters of the TIP4P model potential. J Comput Chem 24(8): 973-981.

Hoover, W. G. 1985. Canonical dynamics: Equilibrium phase-space distributions. Phys Rev A 31(3): 1695-1697.

Humphrey, W., Dalke, A., and Schulten, K. 1996. VMD -visual molecular dynamics. J Mol Graphics 14: 33-38.

Hussain, M. and Anwar, J. 1999. The riddle of resorcinol crystal growth revisited: Molecular dynamics simulations of α-resorcinol crystal−water Interface. J Am Chem Soc 121(37): 8583-8591.

Jorgensen, W. L., Chandrasekhar, J., Madura, J. D., Impey, R. W., and Klein, M. L. 1983. Comparison of simple potential functions for simulating liquid water. J Chem Phys 79(2): 926-935.

Kell, G. S. 1975. Density, thermal expansivity, and compressibility of liquid water from 0.deg. to 150.deg. Correlations and tables for atmospheric pressure and saturation reviewed and expressed on 1968 temperature scale. J Chem Eng Data 20(1): 97-105.

Kofler, A. 1943. Über die stabilen Modifikationen organischer Stoffe. die bei der üblichen Darstellung in einer total oder partiell instabilen Form kristallisieren. Arch. Pharm. Ber. Dtsch. Pharm 281: 8–22.

Langmuir, I. 1917. The constitution and fundamental properties of solids and liquids. II Liquids. 1. J Am Chem Soc 39(9): 1848-1906.

Melchionna, S., Ciccotti, G., Holian, B. L. 1993. Hoover NPT dynamics for systems varying in shape and size. Molec Phys 78: 533–544.

Piana, S. and Gale, J. D. 2005. Understanding the barriers to crystal growth: dynamical simulation of the dissolution and growth of urea from aqueous solution. J Am Chem Soc 127(6): 1975-1982.

Poornachary, S. K., Chow, P. S., and Tan, R. B. H. et al. 2007. Influence of solution speciation of impurities on polymorphic nucleation in glycine. Cryst Growth Des 8(1): 179-185.

Ryckaert, J. P., Ciccotti, G., Berendsen, H. J. C. 1977. Numerical integration of the cartesian equations of motion of a system with constraints: Molecular dynamics of n-alkanes. J Comp Phys 23: 327–341.

Scheel, H. J. 2000. Historical aspects of crystal growth technology. J Cryst Growth 211(1–4): 1-12.

Schmiedel, K. W. and Decker, D. 2000. Resorcinol. In: Ullmann's encyclopedia of industrial chemistry. Weinheim: Wiley-VCH Verlagsgesselschaft

Sharma, S., Vijayakumar, V., Sikka, S. K., and Chidambaram, R. 1985. High pressure phase transitions in organic solids I: α → β transition in resorcinol. Pramana 25(1): 75-79.

Shimon, L. J. W. Vaida, M., Addadi, L., Lahav, M., and Leiserowitz, L. 1990. Molecular recognition at the solid-solution interface: a relay mechanism for the effect of solvent on crystal growth and dissolution. J Am Chem Soc 112(17): 6215-6220.

Smith, W., Todorov, I. T., and Leslie, M. 2005. The DL_POLY molecular dynamics package. Zeitschrift für Kristallographie - Crystalline Materials 220(5-6-2005): 563-566.

Srinivasan, K. and Sherwood, J. N. 2005. Asymmetric growth of α-resorcinol crystals: Comparison of growth from the vapor phase and from aqueous solution. Cryst Growth Des 5(4): 1359-1370.

Srinivasan, K. and Sherwood, J. N. 2011. Asymmetric growth of α-resorcinol crystals: In situ studies of crystal growth from the vapor phase. Cryst Growth Des 11(11): 5010-5018.

Sunakawa, I. 2005. Crystals. growth, morphology and perfection. Cambridge: Cambridge University Press.

van der Spoel, D., et al. 2004. GROMACS user manual version 3.2.

Wahab, M. A. 2009. Essentials of crystallography. Oxford: Alpha Science International Ltd.

Wang. W. S., et al. 1999. Solvent effects and polymorphic transformation of organic nonlinear optical crystal L-pyroglutamic acid in solution growth processes: I. Solvent effects and growth morphology. J Cryst Growth 198–199, Part 1(0): 578-582.

Wells, A. F. 1949. Abnormal and modified crystal growth. Introductory paper. Discuss Faraday Soc 5(0): 197-201.

Weissbuch, I., Popovitz-Biro, R., Lahav, M., and Leiserowitz, L. 1995. Understanding and control of nucleation, growth, habit, dissolution and structure of two- and three-dimensional crystals using `tailor-made' auxiliaries. Acta Crystallogr B 51(2): 115-148.

Weissbuch, I., et al. 2006. Self-poisoning at {011} faces of α-resorcinol crystals may explain its unidirectional growth in the vapor phase: A molecular modeling study. Cryst Growth Des 6(3): 625-628.

Wireko, F. C., et al. 1987. Effect of solvent on the growth of organic crystals. 1. The riddle of .alpha.-resorcinol. J Phys Chem 91(2): 472-481.

Yang, Y., Meng, S., and Wang, E. G. 2006. A molecular dynamics study of hydration and dissolution of NaCl nanocrystal in liquid water. J Phys: Condens Matter 18: 10165-10177.

Yoshino, M., et al. 1999. Contribution of hydrogen bonds to equilibrium αβ transition of Resorcinol. J Phys Chem A 103(15): 2775-2783.

Appendices

Appendix A:

Forcefield parameters for water

```
Water TIP4P
UNITS kJ
molecular types  1

TIP4P water
NUMMOLS 343
ATOMS 4
  ow       15.9994      0.0000    1
  hw       1.00080      0.5200    1
  hw       1.00080      0.5200    1
  mw        0.00000     -1.0400    1
rigid bodies 1
  4    1    2    3    4
FINISH
vdw   1
  ow      ow   lj  0.648520      3.15358
close
```

Appendix B:

Forcefield parameters for dissolution simulation

B-1. Equilibration

B-2. Dissolution simulation

B-1. Equilibration

Alpha Resorcinol Crystal and Water Molecules

units kJ

molecular types 2

Alpha Resorcinol Crystal

NUMMOLS 768

ATOMS 14 mass charge rept frozen

HA 100.80000 0.197 1 0

CA 1201.10000 -0.473 1 0

CA 1201.10000 0.444 1 0

CA 1201.10000 -0.346 1 0

CA 1201.10000 -0.046 1 0

CA 1201.10000 -0.346 1 0

CA 1201.10000 0.444 1 0

OH 1599.94000 -0.523 1 0

OH 1599.94000 -0.523 1 0

HO 100.80000 0.366 1 0

HO 100.80000 0.366 1 0

HA 100.80000 0.159 1 0

HA 100.80000 0.159 1 0

HA 100.80000 0.122 1 0

BONDS 14

harm 2 3 3924.6 1.40

harm 3 4 3924.6 1.40

harm 4 5 3924.6 1.40

harm 5 6 3924.6 1.40

harm 6 7 3924.6 1.40

harm 7 2 3924.6 1.40

harm 1 2 3071.1 1.08

harm 10 8 4627.5 0.96

harm 12 4 3071.1 1.08

harm 14 5 3071.1 1.08

harm 13 6 3071.1 1.08

harm 11 9 4627.5 0.96

harm 8 3 3765.6 1.364

harm 9 7 3765.6 1.364

ANGLES 20

harm 1 2 3 292.880 120.00

harm 1 2 7 292.880 120.00

harm 3 2 7 527.184 120.00

harm 2 3 4 527.184 120.00

harm 8 3 2 585.760 120.00

harm 8 3 4 585.760 120.00

harm 3 4 5 527.184 120.00

harm 12 4 3 292.880 120.00

harm 12 4 5 292.880 120.00

harm 4 5 6 527.184 120.00

harm 14 5 4 292.880 120.00

harm 14 5 6 292.880 120.00

harm 5 6 7 527.184 120.00

harm 13 6 5 292.880 120.00

harm 13 6 7 292.880 120.00

harm 6 7 2 527.184 120.00

harm 9 7 6 585.760 120.00

harm 9 7 2 585.760 120.00

harm 10 8 3 292.880 113.00

harm 11 9 7 292.880 113.00

DIHEDRALS 34

cos 1 2 3 4 15.167 180.00 2

cos 1 2 3 8 15.167 180.00 2

cos 7 2 3 4 15.167 180.00 2

cos 7 2 3 8 15.167 180.00 2

cos 2 3 4 5 15.167 180.00 2

cos 2 3 4 12 15.167 180.00 2

cos 8 3 4 5 15.167 180.00 2

cos 8 3 4 12 15.167 180.00 2

cos 3 4 5 6 15.167 180.00 2

cos 3 4 5 14 15.167 180.00 2

cos 12 4 5 6 15.167 180.00 2

cos 12 4 5 14 15.167 180.00 2

cos 4 5 6 7 15.167 180.00 2

cos 4 5 6 13 15.167 180.00 2

cos 14 5 6 7 15.167 180.00 2

cos 14 5 6 13 15.167 180.00 2

cos 5 6 7 2 15.167 180.00 2

cos 5 6 7 9 15.167 180.00 2

cos 13 6 7 2 15.167 180.00 2

```
cos   13   6   7   9   15.167    180.00      2
cos    6   7   2   3   15.167    180.00      2
cos    6   7   2   1   15.167    180.00      2
cos    9   7   2   3   15.167    180.00      2
cos    9   7   2   1   15.167    180.00      2
cos   10   8   3   4    9.094    180.00      2
cos   10   8   3   2    9.094    180.00      2
cos   11   9   7   2    9.094    180.00      2
cos   11   9   7   6    9.094    180.00      2
harm   2   7   3   1    4.602      0.00
harm   3   2   4   8    4.602      0.00
harm   4   3   5  12    4.602      0.00
harm   5   4   6  14    4.602      0.00
harm   6   5   7  13    4.602      0.00
harm   7   6   2   9    4.602      0.00
finish

TIP4P Water
NUMMOLS 3200
ATOMS 4
  OW      15.9994     0.0000   1
  HW      1.00080     0.5200   1
  HW      1.00080     0.5200   1
  MW      0.00000    -1.0400   1
rigid 1
  4   1   2   3   4
```

```
FINISH
VDW 28
CA      CA      buck  238577.00000   0.27778   1642.70000
CA      OH      buck  234281.83653   0.26515   1358.57930
CA      HO      buck   34641.62684   0.24619    187.93097
CA      HA      buck   53441.60614   0.27258    473.35429
OH      OH      buck  230064.00000   0.25253   1123.60000
OH      HO      buck   34017.96467   0.20861    155.42651
OH      HA      buck   52479.48308   0.25995    391.48313
HO      HO      buck    5030.00000   0.21459     21.50000
HO      HA      buck    7759.77641   0.24099     54.15349
HA      HA      buck   11971.00000   0.26738    136.40000
OW      OW        lj   0.648520      3.153650
OW      HW        lj   0.000000      1.576825
OW      MW        lj   0.000000      1.576825
HW      HW        lj   0.000000      0.000000
HW      MW        lj   0.000000      0.000000
MW      MW        lj   0.000000      0.000000
CA      OW        lj   0.482060      3.276660
CA      HW        lj   0.000000      1.699835
CA      MW        lj   0.000000      1.699835
OH      OW        lj   0.754006      3.110062
OH      HW        lj   0.000000      1.533237
OH      MW        lj   0.000000      1.533237
HO      OW        lj   0.000000      1.576825
HO      HW        lj   0.000000      0.000000
```

HO MW lj 0.000000 0.000000

HA OW lj 0.201325 2.876646

HA HW lj 0.000000 1.299821

HA MW lj 0.000000 1.299821

close

B-2. Dissolution simulation

Alpha Resorcinol Crystal and Water Molecules

units kJ

molecular types 2

Alpha Resorcinol Crystal

NUMMOLS 768

ATOMS 14 mass charge rept frozen

HA	1.00800	0.197	1	0
CA	12.01100	-0.473	1	0
CA	12.01100	0.444	1	0
CA	12.01100	-0.346	1	0
CA	12.01100	-0.046	1	0
CA	12.01100	-0.346	1	0
CA	12.01100	0.444	1	0
OH	15.99940	-0.523	1	0
OH	15.99940	-0.523	1	0
HO	1.00800	0.366	1	0
HO	1.00800	0.366	1	0
HA	1.00800	0.159	1	0
HA	1.00800	0.159	1	0
HA	1.00800	0.122	1	0

BONDS 14

harm 2 3 3924.6 1.40

harm 3 4 3924.6 1.40

harm 4 5 3924.6 1.40

harm 5 6 3924.6 1.40

harm 6 7 3924.6 1.40

harm 7 2 3924.6 1.40

harm 1 2 3071.1 1.08

harm 10 8 4627.5 0.96

harm 12 4 3071.1 1.08

harm 14 5 3071.1 1.08

harm 13 6 3071.1 1.08

harm 11 9 4627.5 0.96

harm 8 3 3765.6 1.364

harm 9 7 3765.6 1.364

ANGLES 20

harm 1 2 3 292.880 120.00

harm 1 2 7 292.880 120.00

harm 3 2 7 527.184 120.00

harm 2 3 4 527.184 120.00

harm 8 3 2 585.760 120.00

harm 8 3 4 585.760 120.00

harm 3 4 5 527.184 120.00

harm 12 4 3 292.880 120.00

harm 12 4 5 292.880 120.00

harm 4 5 6 527.184 120.00

harm 14 5 4 292.880 120.00

harm 14 5 6 292.880 120.00

harm 5 6 7 527.184 120.00

harm 13 6 5 292.880 120.00

harm 13 6 7 292.880 120.00

harm 6 7 2 527.184 120.00

harm 9 7 6 585.760 120.00

harm 9 7 2 585.760 120.00

harm 10 8 3 292.880 113.00

harm 11 9 7 292.880 113.00

DIHEDRALS 34

cos 1 2 3 4 15.167 180.00 2

cos 1 2 3 8 15.167 180.00 2

cos 7 2 3 4 15.167 180.00 2

cos 7 2 3 8 15.167 180.00 2

cos 2 3 4 5 15.167 180.00 2

cos 2 3 4 12 15.167 180.00 2

cos 8 3 4 5 15.167 180.00 2

cos 8 3 4 12 15.167 180.00 2

cos 3 4 5 6 15.167 180.00 2

cos 3 4 5 14 15.167 180.00 2

cos 12 4 5 6 15.167 180.00 2

cos 12 4 5 14 15.167 180.00 2

cos 4 5 6 7 15.167 180.00 2

cos 4 5 6 13 15.167 180.00 2

cos 14 5 6 7 15.167 180.00 2

cos 14 5 6 13 15.167 180.00 2

cos 5 6 7 2 15.167 180.00 2

cos 5 6 7 9 15.167 180.00 2

cos 13 6 7 2 15.167 180.00 2

```
cos   13   6   7   9   15.167    180.00      2
cos    6   7   2   3   15.167    180.00      2
cos    6   7   2   1   15.167    180.00      2
cos    9   7   2   3   15.167    180.00      2
cos    9   7   2   1   15.167    180.00      2
cos   10   8   3   4    9.094    180.00      2
cos   10   8   3   2    9.094    180.00      2
cos   11   9   7   2    9.094    180.00      2
cos   11   9   7   6    9.094    180.00      2
harm   2   7   3   1    4.602      0.00
harm   3   2   4   8    4.602      0.00
harm   4   3   5  12    4.602      0.00
harm   5   4   6  14    4.602      0.00
harm   6   5   7  13    4.602      0.00
harm   7   6   2   9    4.602      0.00
finish

TIP4P Water
NUMMOLS 3200
ATOMS 4
  OW      15.9994     0.0000   1
  HW      1.00080     0.5200   1
  HW      1.00080     0.5200   1
  MW      0.00000    -1.0400   1
rigid 1
  4   1   2   3   4
```

FINISH

VDW 28

CA CA buck 238577.00000 0.27778 1642.70000

CA OH buck 234281.83653 0.26515 1358.57930

CA HO buck 34641.62684 0.24619 187.93097

CA HA buck 53441.60614 0.27258 473.35429

OH OH buck 230064.00000 0.25253 1123.60000

OH HO buck 34017.96467 0.20861 155.42651

OH HA buck 52479.48308 0.25995 391.48313

HO HO buck 5030.00000 0.21459 21.50000

HO HA buck 7759.77641 0.24099 54.15349

HA HA buck 11971.00000 0.26738 136.40000

OW OW lj 0.648520 3.153650

OW HW lj 0.000000 1.576825

OW MW lj 0.000000 1.576825

HW HW lj 0.000000 0.000000

HW MW lj 0.000000 0.000000

MW MW lj 0.000000 0.000000

CA OW lj 0.482060 3.276660

CA HW lj 0.000000 1.699835

CA MW lj 0.000000 1.699835

OH OW lj 0.754006 3.110062

OH HW lj 0.000000 1.533237

OH MW lj 0.000000 1.533237

HO OW lj 0.000000 1.576825

HO HW lj 0.000000 0.000000

```
HO      MW        lj   0.000000      0.000000
HA      OW        lj   0.201325      2.876646
HA      HW        lj   0.000000      1.299821
HA      MW        lj   0.000000      1.299821
close
```

Appendix C:

Forcefield parameters for crystal growth from solution simulation

C-1. Equilibration

C-2. Crystal growth from solution simulation

C-1. Equilibration

Alpha Resorcinol Crystal, Alpha Resorcinol Molecules, and Water Molecules

units kJ

molecular types 3

Alpha Resorcinol Crystal

NUMMOLS 512

ATOMS 14 mass charge rept frozen

HA 100.80000 0.197 1 0

CA 1201.10000 -0.473 1 0

CA 1201.10000 0.444 1 0

CA 1201.10000 -0.346 1 0

CA 1201.10000 -0.046 1 0

CA 1201.10000 -0.346 1 0

CA 1201.10000 0.444 1 0

OH 1599.94000 -0.523 1 0

OH 1599.94000 -0.523 1 0

HO 100.80000 0.366 1 0

HO 100.80000 0.366 1 0

HA 100.80000 0.159 1 0

HA 100.80000 0.159 1 0

HA 100.80000 0.122 1 0

BONDS 14

harm 2 3 3924.6 1.40

harm 3 4 3924.6 1.40

harm 4 5 3924.6 1.40

harm 5 6 3924.6 1.40

harm 6 7 3924.6 1.40

harm 7 2 3924.6 1.40

harm 1 2 3071.1 1.08

harm 10 8 4627.5 0.96

harm 12 4 3071.1 1.08

harm 14 5 3071.1 1.08

harm 13 6 3071.1 1.08

harm 11 9 4627.5 0.96

harm 8 3 3765.6 1.364

harm 9 7 3765.6 1.364

ANGLES 20

harm 1 2 3 292.880 120.00

harm 1 2 7 292.880 120.00

harm 3 2 7 527.184 120.00

harm 2 3 4 527.184 120.00

harm 8 3 2 585.760 120.00

harm 8 3 4 585.760 120.00

harm 3 4 5 527.184 120.00

harm 12 4 3 292.880 120.00

harm 12 4 5 292.880 120.00

harm 4 5 6 527.184 120.00

harm 14 5 4 292.880 120.00

harm 14 5 6 292.880 120.00

harm 5 6 7 527.184 120.00

harm 13 6 5 292.880 120.00

harm 13 6 7 292.880 120.00

harm 6 7 2 527.184 120.00

harm 9 7 6 585.760 120.00

harm 9 7 2 585.760 120.00

harm 10 8 3 292.880 113.00

harm 11 9 7 292.880 113.00

DIHEDRALS 34

cos 1 2 3 4 15.167 180.00 2

cos 1 2 3 8 15.167 180.00 2

cos 7 2 3 4 15.167 180.00 2

cos 7 2 3 8 15.167 180.00 2

cos 2 3 4 5 15.167 180.00 2

cos 2 3 4 12 15.167 180.00 2

cos 8 3 4 5 15.167 180.00 2

cos 8 3 4 12 15.167 180.00 2

cos 3 4 5 6 15.167 180.00 2

cos 3 4 5 14 15.167 180.00 2

cos 12 4 5 6 15.167 180.00 2

cos 12 4 5 14 15.167 180.00 2

cos 4 5 6 7 15.167 180.00 2

cos 4 5 6 13 15.167 180.00 2

cos 14 5 6 7 15.167 180.00 2

cos 14 5 6 13 15.167 180.00 2

cos 5 6 7 2 15.167 180.00 2

cos 5 6 7 9 15.167 180.00 2

cos 13 6 7 2 15.167 180.00 2

cos 13 6 7 9 15.167 180.00 2

cos 6 7 2 3 15.167 180.00 2

cos 6 7 2 1 15.167 180.00 2

cos 9 7 2 3 15.167 180.00 2

cos 9 7 2 1 15.167 180.00 2

cos 10 8 3 4 9.094 180.00 2

cos 10 8 3 2 9.094 180.00 2

cos 11 9 7 2 9.094 180.00 2

cos 11 9 7 6 9.094 180.00 2

harm 2 7 3 1 4.602 0.00

harm 3 2 4 8 4.602 0.00

harm 4 3 5 12 4.602 0.00

harm 5 4 6 14 4.602 0.00

harm 6 5 7 13 4.602 0.00

harm 7 6 2 9 4.602 0.00

finish
’

Alpha Resorcinol Molecules

NUMMOLS 549

ATOMS 14 mass charge rept frozen

HA 1.00800 0.197 1 0

CA 12.01100 -0.473 1 0

CA 12.01100 0.444 1 0

CA 12.01100 -0.346 1 0

CA 12.01100 -0.046 1 0

CA 12.01100 -0.346 1 0

```
   CA     12.01100     0.444     1    0
   OH     15.99940    -0.523     1    0
   OH     15.99940    -0.523     1    0
   HO      1.00800     0.366     1    0
   HO      1.00800     0.366     1    0
   HA      1.00800     0.159     1    0
   HA      1.00800     0.159     1    0
   HA      1.00800     0.122     1    0
BONDS 14
harm   2    3   3924.6      1.40
harm   3    4   3924.6      1.40
harm   4    5   3924.6      1.40
harm   5    6   3924.6      1.40
harm   6    7   3924.6      1.40
harm   7    2   3924.6      1.40
harm   1    2   3071.1      1.08
harm  10    8   4627.5      0.96
harm  12    4   3071.1      1.08
harm  14    5   3071.1      1.08
harm  13    6   3071.1      1.08
harm  11    9   4627.5      0.96
harm   8    3   3765.6      1.364
harm   9    7   3765.6      1.364
ANGLES 20
harm   1    2    3   292.880     120.00
harm   1    2    7   292.880     120.00
```

harm 3 2 7 527.184 120.00

harm 2 3 4 527.184 120.00

harm 8 3 2 585.760 120.00

harm 8 3 4 585.760 120.00

harm 3 4 5 527.184 120.00

harm 12 4 3 292.880 120.00

harm 12 4 5 292.880 120.00

harm 4 5 6 527.184 120.00

harm 14 5 4 292.880 120.00

harm 14 5 6 292.880 120.00

harm 5 6 7 527.184 120.00

harm 13 6 5 292.880 120.00

harm 13 6 7 292.880 120.00

harm 6 7 2 527.184 120.00

harm 9 7 6 585.760 120.00

harm 9 7 2 585.760 120.00

harm 10 8 3 292.880 113.00

harm 11 9 7 292.880 113.00

DIHEDRALS 34

cos 1 2 3 4 15.167 180.00 2

cos 1 2 3 8 15.167 180.00 2

cos 7 2 3 4 15.167 180.00 2

cos 7 2 3 8 15.167 180.00 2

cos 2 3 4 5 15.167 180.00 2

cos 2 3 4 12 15.167 180.00 2

cos 8 3 4 5 15.167 180.00 2

```
cos    8   3   4  12   15.167    180.00       2
cos    3   4   5   6   15.167    180.00       2
cos    3   4   5  14   15.167    180.00       2
cos   12   4   5   6   15.167    180.00       2
cos   12   4   5  14   15.167    180.00       2
cos    4   5   6   7   15.167    180.00       2
cos    4   5   6  13   15.167    180.00       2
cos   14   5   6   7   15.167    180.00       2
cos   14   5   6  13   15.167    180.00       2
cos    5   6   7   2   15.167    180.00       2
cos    5   6   7   9   15.167    180.00       2
cos   13   6   7   2   15.167    180.00       2
cos   13   6   7   9   15.167    180.00       2
cos    6   7   2   3   15.167    180.00       2
cos    6   7   2   1   15.167    180.00       2
cos    9   7   2   3   15.167    180.00       2
cos    9   7   2   1   15.167    180.00       2
cos   10   8   3   4    9.094    180.00       2
cos   10   8   3   2    9.094    180.00       2
cos   11   9   7   2    9.094    180.00       2
cos   11   9   7   6    9.094    180.00       2
harm   2   7   3   1    4.602      0.00
harm   3   2   4   8    4.602      0.00
harm   4   3   5  12    4.602      0.00
harm   5   4   6  14    4.602      0.00
harm   6   5   7  13    4.602      0.00
```

harm 7 6 2 9 4.602 0.00

finish

TIP4P Water

NUMMOLS 2122

ATOMS 4

OW 15.9994 0.0000 1

HW 1.00080 0.5200 1

HW 1.00080 0.5200 1

MW 0.00000 -1.0400 1

rigid 1

4 1 2 3 4

FINISH

VDW 28

CA CA buck 238577.00000 0.27778 1642.70000

CA OH buck 234281.83653 0.26515 1358.57930

CA HO buck 34641.62684 0.24619 187.93097

CA HA buck 53441.60614 0.27258 473.35429

OH OH buck 230064.00000 0.25253 1123.60000

OH HO buck 34017.96467 0.20861 155.42651

OH HA buck 52479.48308 0.25995 391.48313

HO HO buck 5030.00000 0.21459 21.50000

HO HA buck 7759.77641 0.24099 54.15349

HA HA buck 11971.00000 0.26738 136.40000

OW OW lj 0.648520 3.153650

OW HW lj 0.000000 1.576825

```
OW      MW        lj   0.000000      1.576825
HW      HW        lj   0.000000      0.000000
HW      MW        lj   0.000000      0.000000
MW      MW        lj   0.000000      0.000000
CA      OW        lj   0.482060      3.276660
CA      HW        lj   0.000000      1.699835
CA      MW        lj   0.000000      1.699835
OH      OW        lj   0.754006      3.110062
OH      HW        lj   0.000000      1.533237
OH      MW        lj   0.000000      1.533237
HO      OW        lj   0.000000      1.576825
HO      HW        lj   0.000000      0.000000
HO      MW        lj   0.000000      0.000000
HA      OW        lj   0.201325      2.876646
HA      HW        lj   0.000000      1.299821
HA      MW        lj   0.000000      1.299821
close
```

C-2. Crystal growth from solution simulation

Alpha Resorcinol Crystal, Alpha Resorcinol Molecules, and Water Molecules

units kJ

molecular types 3

Alpha Resorcinol Crystal

NUMMOLS 512

ATOMS 14 mass charge rept frozen

HA	1.00800	0.197	1	0
CA	12.01100	-0.473	1	0
CA	12.01100	0.444	1	0
CA	12.01100	-0.346	1	0
CA	12.01100	-0.046	1	0
CA	12.01100	-0.346	1	0
CA	12.01100	0.444	1	0
OH	15.99940	-0.523	1	0
OH	15.99940	-0.523	1	0
HO	1.00800	0.366	1	0
HO	1.00800	0.366	1	0
HA	1.00800	0.159	1	0
HA	1.00800	0.159	1	0
HA	1.00800	0.122	1	0

BONDS 14

harm 2 3 3924.6 1.40

harm 3 4 3924.6 1.40

harm 4 5 3924.6 1.40

harm 5 6 3924.6 1.40

harm 6 7 3924.6 1.40

harm 7 2 3924.6 1.40

harm 1 2 3071.1 1.08

harm 10 8 4627.5 0.96

harm 12 4 3071.1 1.08

harm 14 5 3071.1 1.08

harm 13 6 3071.1 1.08

harm 11 9 4627.5 0.96

harm 8 3 3765.6 1.364

harm 9 7 3765.6 1.364

ANGLES 20

harm 1 2 3 292.880 120.00

harm 1 2 7 292.880 120.00

harm 3 2 7 527.184 120.00

harm 2 3 4 527.184 120.00

harm 8 3 2 585.760 120.00

harm 8 3 4 585.760 120.00

harm 3 4 5 527.184 120.00

harm 12 4 3 292.880 120.00

harm 12 4 5 292.880 120.00

harm 4 5 6 527.184 120.00

harm 14 5 4 292.880 120.00

harm 14 5 6 292.880 120.00

harm 5 6 7 527.184 120.00

harm 13 6 5 292.880 120.00

harm 13 6 7 292.880 120.00

harm 6 7 2 527.184 120.00

harm 9 7 6 585.760 120.00

harm 9 7 2 585.760 120.00

harm 10 8 3 292.880 113.00

harm 11 9 7 292.880 113.00

DIHEDRALS 34

cos 1 2 3 4 15.167 180.00 2

cos 1 2 3 8 15.167 180.00 2

cos 7 2 3 4 15.167 180.00 2

cos 7 2 3 8 15.167 180.00 2

cos 2 3 4 5 15.167 180.00 2

cos 2 3 4 12 15.167 180.00 2

cos 8 3 4 5 15.167 180.00 2

cos 8 3 4 12 15.167 180.00 2

cos 3 4 5 6 15.167 180.00 2

cos 3 4 5 14 15.167 180.00 2

cos 12 4 5 6 15.167 180.00 2

cos 12 4 5 14 15.167 180.00 2

cos 4 5 6 7 15.167 180.00 2

cos 4 5 6 13 15.167 180.00 2

cos 14 5 6 7 15.167 180.00 2

cos 14 5 6 13 15.167 180.00 2

cos 5 6 7 2 15.167 180.00 2

cos 5 6 7 9 15.167 180.00 2

cos 13 6 7 2 15.167 180.00 2

cos 13 6 7 9 15.167 180.00 2

cos 6 7 2 3 15.167 180.00 2

cos 6 7 2 1 15.167 180.00 2

cos 9 7 2 3 15.167 180.00 2

cos 9 7 2 1 15.167 180.00 2

cos 10 8 3 4 9.094 180.00 2

cos 10 8 3 2 9.094 180.00 2

cos 11 9 7 2 9.094 180.00 2

cos 11 9 7 6 9.094 180.00 2

harm 2 7 3 1 4.602 0.00

harm 3 2 4 8 4.602 0.00

harm 4 3 5 12 4.602 0.00

harm 5 4 6 14 4.602 0.00

harm 6 5 7 13 4.602 0.00

harm 7 6 2 9 4.602 0.00

finish

Alpha Resorcinol Molecules

NUMMOLS 549

ATOMS 14 mass charge rept frozen

HA 1.00800 0.197 1 0

CA 12.01100 -0.473 1 0

CA 12.01100 0.444 1 0

CA 12.01100 -0.346 1 0

CA 12.01100 -0.046 1 0

CA 12.01100 -0.346 1 0

CA 12.01100 0.444 1 0

OH 15.99940 -0.523 1 0

OH 15.99940 -0.523 1 0

HO 1.00800 0.366 1 0

HO 1.00800 0.366 1 0

HA 1.00800 0.159 1 0

HA 1.00800 0.159 1 0

HA 1.00800 0.122 1 0

BONDS 14

harm 2 3 3924.6 1.40

harm 3 4 3924.6 1.40

harm 4 5 3924.6 1.40

harm 5 6 3924.6 1.40

harm 6 7 3924.6 1.40

harm 7 2 3924.6 1.40

harm 1 2 3071.1 1.08

harm 10 8 4627.5 0.96

harm 12 4 3071.1 1.08

harm 14 5 3071.1 1.08

harm 13 6 3071.1 1.08

harm 11 9 4627.5 0.96

harm 8 3 3765.6 1.364

harm 9 7 3765.6 1.364

ANGLES 20

harm 1 2 3 292.880 120.00

harm 1 2 7 292.880 120.00

harm 3 2 7 527.184 120.00

harm 2 3 4 527.184 120.00

harm 8 3 2 585.760 120.00

harm 8 3 4 585.760 120.00

harm 3 4 5 527.184 120.00

harm 12 4 3 292.880 120.00

harm 12 4 5 292.880 120.00

harm 4 5 6 527.184 120.00

harm 14 5 4 292.880 120.00

harm 14 5 6 292.880 120.00

harm 5 6 7 527.184 120.00

harm 13 6 5 292.880 120.00

harm 13 6 7 292.880 120.00

harm 6 7 2 527.184 120.00

harm 9 7 6 585.760 120.00

harm 9 7 2 585.760 120.00

harm 10 8 3 292.880 113.00

harm 11 9 7 292.880 113.00

DIHEDRALS 34

cos 1 2 3 4 15.167 180.00 2

cos 1 2 3 8 15.167 180.00 2

cos 7 2 3 4 15.167 180.00 2

cos 7 2 3 8 15.167 180.00 2

cos 2 3 4 5 15.167 180.00 2

cos 2 3 4 12 15.167 180.00 2

cos 8 3 4 5 15.167 180.00 2

```
cos     8    3    4   12    15.167     180.00       2
cos     3    4    5    6    15.167     180.00       2
cos     3    4    5   14    15.167     180.00       2
cos    12    4    5    6    15.167     180.00       2
cos    12    4    5   14    15.167     180.00       2
cos     4    5    6    7    15.167     180.00       2
cos     4    5    6   13    15.167     180.00       2
cos    14    5    6    7    15.167     180.00       2
cos    14    5    6   13    15.167     180.00       2
cos     5    6    7    2    15.167     180.00       2
cos     5    6    7    9    15.167     180.00       2
cos    13    6    7    2    15.167     180.00       2
cos    13    6    7    9    15.167     180.00       2
cos     6    7    2    3    15.167     180.00       2
cos     6    7    2    1    15.167     180.00       2
cos     9    7    2    3    15.167     180.00       2
cos     9    7    2    1    15.167     180.00       2
cos    10    8    3    4     9.094     180.00       2
cos    10    8    3    2     9.094     180.00       2
cos    11    9    7    2     9.094     180.00       2
cos    11    9    7    6     9.094     180.00       2
harm    2    7    3    1     4.602       0.00
harm    3    2    4    8     4.602       0.00
harm    4    3    5   12     4.602       0.00
harm    5    4    6   14     4.602       0.00
harm    6    5    7   13     4.602       0.00
```

harm 7 6 2 9 4.602 0.00

finish

TIP4P Water

NUMMOLS 2122

ATOMS 4

OW 15.9994 0.0000 1

HW 1.00080 0.5200 1

HW 1.00080 0.5200 1

MW 0.00000 -1.0400 1

rigid 1

4 1 2 3 4

FINISH

VDW 28

CA CA buck 238577.00000 0.27778 1642.70000

CA OH buck 234281.83653 0.26515 1358.57930

CA HO buck 34641.62684 0.24619 187.93097

CA HA buck 53441.60614 0.27258 473.35429

OH OH buck 230064.00000 0.25253 1123.60000

OH HO buck 34017.96467 0.20861 155.42651

OH HA buck 52479.48308 0.25995 391.48313

HO HO buck 5030.00000 0.21459 21.50000

HO HA buck 7759.77641 0.24099 54.15349

HA HA buck 11971.00000 0.26738 136.40000

OW OW lj 0.648520 3.153650

OW HW lj 0.000000 1.576825

OW MW lj 0.000000 1.576825

HW HW lj 0.000000 0.000000

HW MW lj 0.000000 0.000000

MW MW lj 0.000000 0.000000

CA OW lj 0.482060 3.276660

CA HW lj 0.000000 1.699835

CA MW lj 0.000000 1.699835

OH OW lj 0.754006 3.110062

OH HW lj 0.000000 1.533237

OH MW lj 0.000000 1.533237

HO OW lj 0.000000 1.576825

HO HW lj 0.000000 0.000000

HO MW lj 0.000000 0.000000

HA OW lj 0.201325 2.876646

HA HW lj 0.000000 1.299821

HA MW lj 0.000000 1.299821

close

Appendix D:

Forcefield parameters for crystal growth from vapour simulation

Alpha Resorcinol Crystal and Alpha Resorcinol Molecules

units kJ

molecular types 2

Alpha Resorcinol Crystal

NUMMOLS 3072

ATOMS 14 mass charge rept frozen

HA	1.00800	0.197	1	0
CA	12.01100	-0.473	1	0
CA	12.01100	0.444	1	0
CA	12.01100	-0.346	1	0
CA	12.01100	-0.046	1	0
CA	12.01100	-0.346	1	0
CA	12.01100	0.444	1	0
OH	15.99940	-0.523	1	0
OH	15.99940	-0.523	1	0
HO	1.00800	0.366	1	0
HO	1.00800	0.366	1	0
HA	1.00800	0.159	1	0
HA	1.00800	0.159	1	0
HA	1.00800	0.122	1	0

CONSTRAINTS 14

2	3	1.40
3	4	1.40
4	5	1.40
5	6	1.40

6 7 1.40

7 2 1.40

1 2 1.08

10 8 0.96

12 4 1.08

14 5 1.08

13 6 1.08

11 9 0.96

8 3 1.364

9 7 1.364

ANGLES 20

harm 1 2 3 292.880 120.00

harm 1 2 7 292.880 120.00

harm 3 2 7 527.184 120.00

harm 2 3 4 527.184 120.00

harm 8 3 2 585.760 120.00

harm 8 3 4 585.760 120.00

harm 3 4 5 527.184 120.00

harm 12 4 3 292.880 120.00

harm 12 4 5 292.880 120.00

harm 4 5 6 527.184 120.00

harm 14 5 4 292.880 120.00

harm 14 5 6 292.880 120.00

harm 5 6 7 527.184 120.00

harm 13 6 5 292.880 120.00

harm 13 6 7 292.880 120.00

harm 6 7 2 527.184 120.00

harm 9 7 6 585.760 120.00

harm 9 7 2 585.760 120.00

harm 10 8 3 292.880 113.00

harm 11 9 7 292.880 113.00

DIHEDRALS 34

cos 1 2 3 4 15.167 180.00 2

cos 1 2 3 8 15.167 180.00 2

cos 7 2 3 4 15.167 180.00 2

cos 7 2 3 8 15.167 180.00 2

cos 2 3 4 5 15.167 180.00 2

cos 2 3 4 12 15.167 180.00 2

cos 8 3 4 5 15.167 180.00 2

cos 8 3 4 12 15.167 180.00 2

cos 3 4 5 6 15.167 180.00 2

cos 3 4 5 14 15.167 180.00 2

cos 12 4 5 6 15.167 180.00 2

cos 12 4 5 14 15.167 180.00 2

cos 4 5 6 7 15.167 180.00 2

cos 4 5 6 13 15.167 180.00 2

cos 14 5 6 7 15.167 180.00 2

cos 14 5 6 13 15.167 180.00 2

cos 5 6 7 2 15.167 180.00 2

cos 5 6 7 9 15.167 180.00 2

cos 13 6 7 2 15.167 180.00 2

cos 13 6 7 9 15.167 180.00 2

cos 6 7 2 3 15.167 180.00 2

cos 6 7 2 1 15.167 180.00 2

cos 9 7 2 3 15.167 180.00 2

cos 9 7 2 1 15.167 180.00 2

cos 10 8 3 4 9.094 180.00 2

cos 10 8 3 2 9.094 180.00 2

cos 11 9 7 2 9.094 180.00 2

cos 11 9 7 6 9.094 180.00 2

harm 2 7 3 1 4.602 0.00

harm 3 2 4 8 4.602 0.00

harm 4 3 5 12 4.602 0.00

harm 5 4 6 14 4.602 0.00

harm 6 5 7 13 4.602 0.00

harm 7 6 2 9 4.602 0.00

finish

Alpha Resorcinol Molecules

NUMMOLS 1500

ATOMS 14 mass charge rept frozen

HA 1.00800 0.197 1 0

CA 12.01100 -0.473 1 0

CA 12.01100 0.444 1 0

CA 12.01100 -0.346 1 0

CA 12.01100 -0.046 1 0

CA 12.01100 -0.346 1 0

CA 12.01100 0.444 1 0

```
   OH     15.99940    -0.523     1    0
   OH     15.99940    -0.523     1    0
   HO      1.00800     0.366     1    0
   HO      1.00800     0.366     1    0
   HA      1.00800     0.159     1    0
   HA      1.00800     0.159     1    0
   HA      1.00800     0.122     1    0
CONSTRAINTS 14
   2    3    1.40
   3    4    1.40
   4    5    1.40
   5    6    1.40
   6    7    1.40
   7    2    1.40
   1    2    1.08
  10    8    0.96
  12    4    1.08
  14    5    1.08
  13    6    1.08
  11    9    0.96
   8    3    1.364
   9    7    1.364
ANGLES 20
harm   1    2    3   292.880     120.00
harm   1    2    7   292.880     120.00
harm   3    2    7   527.184     120.00
```

harm 2 3 4 527.184 120.00

harm 8 3 2 585.760 120.00

harm 8 3 4 585.760 120.00

harm 3 4 5 527.184 120.00

harm 12 4 3 292.880 120.00

harm 12 4 5 292.880 120.00

harm 4 5 6 527.184 120.00

harm 14 5 4 292.880 120.00

harm 14 5 6 292.880 120.00

harm 5 6 7 527.184 120.00

harm 13 6 5 292.880 120.00

harm 13 6 7 292.880 120.00

harm 6 7 2 527.184 120.00

harm 9 7 6 585.760 120.00

harm 9 7 2 585.760 120.00

harm 10 8 3 292.880 113.00

harm 11 9 7 292.880 113.00

DIHEDRALS 34

cos 1 2 3 4 15.167 180.00 2

cos 1 2 3 8 15.167 180.00 2

cos 7 2 3 4 15.167 180.00 2

cos 7 2 3 8 15.167 180.00 2

cos 2 3 4 5 15.167 180.00 2

cos 2 3 4 12 15.167 180.00 2

cos 8 3 4 5 15.167 180.00 2

cos 8 3 4 12 15.167 180.00 2

```
cos    3    4    5    6    15.167     180.00       2
cos    3    4    5   14    15.167     180.00       2
cos   12    4    5    6    15.167     180.00       2
cos   12    4    5   14    15.167     180.00       2
cos    4    5    6    7    15.167     180.00       2
cos    4    5    6   13    15.167     180.00       2
cos   14    5    6    7    15.167     180.00       2
cos   14    5    6   13    15.167     180.00       2
cos    5    6    7    2    15.167     180.00       2
cos    5    6    7    9    15.167     180.00       2
cos   13    6    7    2    15.167     180.00       2
cos   13    6    7    9    15.167     180.00       2
cos    6    7    2    3    15.167     180.00       2
cos    6    7    2    1    15.167     180.00       2
cos    9    7    2    3    15.167     180.00       2
cos    9    7    2    1    15.167     180.00       2
cos   10    8    3    4     9.094     180.00       2
cos   10    8    3    2     9.094     180.00       2
cos   11    9    7    2     9.094     180.00       2
cos   11    9    7    6     9.094     180.00       2
harm   2    7    3    1     4.602       0.00
harm   3    2    4    8     4.602       0.00
harm   4    3    5   12     4.602       0.00
harm   5    4    6   14     4.602       0.00
harm   6    5    7   13     4.602       0.00
harm   7    6    2    9     4.602       0.00
```

finish

VDW 10

CA CA buck 238577.00000 0.27778 1642.70000

CA OH buck 234281.83653 0.26515 1358.57930

CA HO buck 34641.62684 0.24619 187.93097

CA HA buck 53441.60614 0.27258 473.35429

OH OH buck 230064.00000 0.25253 1123.60000

OH HO buck 34017.96467 0.20861 155.42651

OH HA buck 52479.48308 0.25995 391.48313

HO HO buck 5030.00000 0.21459 21.50000

HO HA buck 7759.77641 0.24099 54.15349

HA HA buck 11971.00000 0.26738 136.40000

close

Appendix E:

Forcefield parameters for crystal growth from melt simulation

E-1. Equilibration

E-2. Crystal growth from melt simulation

E-1. Equilibration

Alpha Resorcinol Crystal and Alpha Resorcinol Molecules

units kJ

molecular types 2

Alpha Resorcinol Crystal

NUMMOLS 3072

ATOMS 14 mass charge rept frozen

HA	100.800	0.197	1	0
CA	1201.100	-0.473	1	0
CA	1201.100	0.444	1	0
CA	1201.100	-0.346	1	0
CA	1201.100	-0.046	1	0
CA	1201.100	-0.346	1	0
CA	1201.100	0.444	1	0
OH	1599.940	-0.523	1	0
OH	1599.940	-0.523	1	0
HO	100.800	0.366	1	0
HO	100.800	0.366	1	0
HA	100.800	0.159	1	0
HA	100.800	0.159	1	0
HA	100.800	0.122	1	0

CONSTRAINTS 14

2	3	1.40
3	4	1.40
4	5	1.40

5 6 1.40

6 7 1.40

7 2 1.40

1 2 1.08

10 8 0.96

12 4 1.08

14 5 1.08

13 6 1.08

11 9 0.96

8 3 1.364

9 7 1.364

ANGLES 20

harm 1 2 3 292.880 120.00

harm 1 2 7 292.880 120.00

harm 3 2 7 527.184 120.00

harm 2 3 4 527.184 120.00

harm 8 3 2 585.760 120.00

harm 8 3 4 585.760 120.00

harm 3 4 5 527.184 120.00

harm 12 4 3 292.880 120.00

harm 12 4 5 292.880 120.00

harm 4 5 6 527.184 120.00

harm 14 5 4 292.880 120.00

harm 14 5 6 292.880 120.00

harm 5 6 7 527.184 120.00

harm 13 6 5 292.880 120.00

harm 13 6 7 292.880 120.00

harm 6 7 2 527.184 120.00

harm 9 7 6 585.760 120.00

harm 9 7 2 585.760 120.00

harm 10 8 3 292.880 113.00

harm 11 9 7 292.880 113.00

DIHEDRALS 34

cos 1 2 3 4 15.167 180.00 2

cos 1 2 3 8 15.167 180.00 2

cos 7 2 3 4 15.167 180.00 2

cos 7 2 3 8 15.167 180.00 2

cos 2 3 4 5 15.167 180.00 2

cos 2 3 4 12 15.167 180.00 2

cos 8 3 4 5 15.167 180.00 2

cos 8 3 4 12 15.167 180.00 2

cos 3 4 5 6 15.167 180.00 2

cos 3 4 5 14 15.167 180.00 2

cos 12 4 5 6 15.167 180.00 2

cos 12 4 5 14 15.167 180.00 2

cos 4 5 6 7 15.167 180.00 2

cos 4 5 6 13 15.167 180.00 2

cos 14 5 6 7 15.167 180.00 2

cos 14 5 6 13 15.167 180.00 2

cos 5 6 7 2 15.167 180.00 2

cos 5 6 7 9 15.167 180.00 2

cos 13 6 7 2 15.167 180.00 2

cos 13 6 7 9 15.167 180.00 2

cos 6 7 2 3 15.167 180.00 2

cos 6 7 2 1 15.167 180.00 2

cos 9 7 2 3 15.167 180.00 2

cos 9 7 2 1 15.167 180.00 2

cos 10 8 3 4 9.094 180.00 2

cos 10 8 3 2 9.094 180.00 2

cos 11 9 7 2 9.094 180.00 2

cos 11 9 7 6 9.094 180.00 2

harm 2 7 3 1 4.602 0.00

harm 3 2 4 8 4.602 0.00

harm 4 3 5 12 4.602 0.00

harm 5 4 6 14 4.602 0.00

harm 6 5 7 13 4.602 0.00

harm 7 6 2 9 4.602 0.00

finish

Alpha Resorcinol Molecules

NUMMOLS 2500

ATOMS 14 mass charge rept frozen

HA 1.00800 0.197 1 0

CA 12.01100 -0.473 1 0

CA 12.01100 0.444 1 0

CA 12.01100 -0.346 1 0

CA 12.01100 -0.046 1 0

CA 12.01100 -0.346 1 0

```
   CA     12.01100     0.444     1    0
   OH     15.99940    -0.523     1    0
   OH     15.99940    -0.523     1    0
   HO      1.00800     0.366     1    0
   HO      1.00800     0.366     1    0
   HA      1.00800     0.159     1    0
   HA      1.00800     0.159     1    0
   HA      1.00800     0.122     1    0
CONSTRAINTS 14
   2    3    1.40
   3    4    1.40
   4    5    1.40
   5    6    1.40
   6    7    1.40
   7    2    1.40
   1    2    1.08
  10    8    0.96
  12    4    1.08
  14    5    1.08
  13    6    1.08
  11    9    0.96
   8    3    1.364
   9    7    1.364
ANGLES 20
harm   1    2    3   292.880     120.00
harm   1    2    7   292.880     120.00
```

harm 3 2 7 527.184 120.00

harm 2 3 4 527.184 120.00

harm 8 3 2 585.760 120.00

harm 8 3 4 585.760 120.00

harm 3 4 5 527.184 120.00

harm 12 4 3 292.880 120.00

harm 12 4 5 292.880 120.00

harm 4 5 6 527.184 120.00

harm 14 5 4 292.880 120.00

harm 14 5 6 292.880 120.00

harm 5 6 7 527.184 120.00

harm 13 6 5 292.880 120.00

harm 13 6 7 292.880 120.00

harm 6 7 2 527.184 120.00

harm 9 7 6 585.760 120.00

harm 9 7 2 585.760 120.00

harm 10 8 3 292.880 113.00

harm 11 9 7 292.880 113.00

DIHEDRALS 34

cos 1 2 3 4 15.167 180.00 2

cos 1 2 3 8 15.167 180.00 2

cos 7 2 3 4 15.167 180.00 2

cos 7 2 3 8 15.167 180.00 2

cos 2 3 4 5 15.167 180.00 2

cos 2 3 4 12 15.167 180.00 2

cos 8 3 4 5 15.167 180.00 2

```
cos    8   3   4  12   15.167    180.00       2
cos    3   4   5   6   15.167    180.00       2
cos    3   4   5  14   15.167    180.00       2
cos   12   4   5   6   15.167    180.00       2
cos   12   4   5  14   15.167    180.00       2
cos    4   5   6   7   15.167    180.00       2
cos    4   5   6  13   15.167    180.00       2
cos   14   5   6   7   15.167    180.00       2
cos   14   5   6  13   15.167    180.00       2
cos    5   6   7   2   15.167    180.00       2
cos    5   6   7   9   15.167    180.00       2
cos   13   6   7   2   15.167    180.00       2
cos   13   6   7   9   15.167    180.00       2
cos    6   7   2   3   15.167    180.00       2
cos    6   7   2   1   15.167    180.00       2
cos    9   7   2   3   15.167    180.00       2
cos    9   7   2   1   15.167    180.00       2
cos   10   8   3   4    9.094    180.00       2
cos   10   8   3   2    9.094    180.00       2
cos   11   9   7   2    9.094    180.00       2
cos   11   9   7   6    9.094    180.00       2
harm   2   7   3   1    4.602      0.00
harm   3   2   4   8    4.602      0.00
harm   4   3   5  12    4.602      0.00
harm   5   4   6  14    4.602      0.00
harm   6   5   7  13    4.602      0.00
```

harm 7 6 2 9 4.602 0.00

finish

VDW 10

CA CA buck 238577.00000 0.27778 1642.70000

CA OH buck 234281.83653 0.26515 1358.57930

CA HO buck 34641.62684 0.24619 187.93097

CA HA buck 53441.60614 0.27258 473.35429

OH OH buck 230064.00000 0.25253 1123.60000

OH HO buck 34017.96467 0.20861 155.42651

OH HA buck 52479.48308 0.25995 391.48313

HO HO buck 5030.00000 0.21459 21.50000

HO HA buck 7759.77641 0.24099 54.15349

HA HA buck 11971.00000 0.26738 136.40000

Close

E-2. Crystal growth in melt simulation

Alpha Resorcinol Crystal

units kJ

molecular types 2

Alpha Resorcinol Crystal

NUMMOLS 3072

ATOMS 14 mass charge rept frozen

HA	1.00800	0.197	1	0
CA	12.01100	-0.473	1	0
CA	12.01100	0.444	1	0
CA	12.01100	-0.346	1	0
CA	12.01100	-0.046	1	0
CA	12.01100	-0.346	1	0
CA	12.01100	0.444	1	0
OH	15.99940	-0.523	1	0
OH	15.99940	-0.523	1	0
HO	1.00800	0.366	1	0
HO	1.00800	0.366	1	0
HA	1.00800	0.159	1	0
HA	1.00800	0.159	1	0
HA	1.00800	0.122	1	0

CONSTRAINTS 14

2	3	1.40
3	4	1.40
4	5	1.40

5 6 1.40

6 7 1.40

7 2 1.40

1 2 1.08

10 8 0.96

12 4 1.08

14 5 1.08

13 6 1.08

11 9 0.96

8 3 1.364

9 7 1.364

ANGLES 20

harm 1 2 3 292.880 120.00

harm 1 2 7 292.880 120.00

harm 3 2 7 527.184 120.00

harm 2 3 4 527.184 120.00

harm 8 3 2 585.760 120.00

harm 8 3 4 585.760 120.00

harm 3 4 5 527.184 120.00

harm 12 4 3 292.880 120.00

harm 12 4 5 292.880 120.00

harm 4 5 6 527.184 120.00

harm 14 5 4 292.880 120.00

harm 14 5 6 292.880 120.00

harm 5 6 7 527.184 120.00

harm 13 6 5 292.880 120.00

harm 13 6 7 292.880 120.00

harm 6 7 2 527.184 120.00

harm 9 7 6 585.760 120.00

harm 9 7 2 585.760 120.00

harm 10 8 3 292.880 113.00

harm 11 9 7 292.880 113.00

DIHEDRALS 34

cos 1 2 3 4 15.167 180.00 2

cos 1 2 3 8 15.167 180.00 2

cos 7 2 3 4 15.167 180.00 2

cos 7 2 3 8 15.167 180.00 2

cos 2 3 4 5 15.167 180.00 2

cos 2 3 4 12 15.167 180.00 2

cos 8 3 4 5 15.167 180.00 2

cos 8 3 4 12 15.167 180.00 2

cos 3 4 5 6 15.167 180.00 2

cos 3 4 5 14 15.167 180.00 2

cos 12 4 5 6 15.167 180.00 2

cos 12 4 5 14 15.167 180.00 2

cos 4 5 6 7 15.167 180.00 2

cos 4 5 6 13 15.167 180.00 2

cos 14 5 6 7 15.167 180.00 2

cos 14 5 6 13 15.167 180.00 2

cos 5 6 7 2 15.167 180.00 2

cos 5 6 7 9 15.167 180.00 2

cos 13 6 7 2 15.167 180.00 2

cos 13 6 7 9 15.167 180.00 2

cos 6 7 2 3 15.167 180.00 2

cos 6 7 2 1 15.167 180.00 2

cos 9 7 2 3 15.167 180.00 2

cos 9 7 2 1 15.167 180.00 2

cos 10 8 3 4 9.094 180.00 2

cos 10 8 3 2 9.094 180.00 2

cos 11 9 7 2 9.094 180.00 2

cos 11 9 7 6 9.094 180.00 2

harm 2 7 3 1 4.602 0.00

harm 3 2 4 8 4.602 0.00

harm 4 3 5 12 4.602 0.00

harm 5 4 6 14 4.602 0.00

harm 6 5 7 13 4.602 0.00

harm 7 6 2 9 4.602 0.00

finish

Alpha Resorcinol Molecules

NUMMOLS 2500

ATOMS 14 mass charge rept frozen

HA 1.00800 0.197 1 0

CA 12.01100 -0.473 1 0

CA 12.01100 0.444 1 0

CA 12.01100 -0.346 1 0

CA 12.01100 -0.046 1 0

CA 12.01100 -0.346 1 0

CA 12.01100 0.444 1 0

OH 15.99940 -0.523 1 0

OH 15.99940 -0.523 1 0

HO 1.00800 0.366 1 0

HO 1.00800 0.366 1 0

HA 1.00800 0.159 1 0

HA 1.00800 0.159 1 0

HA 1.00800 0.122 1 0

CONSTRAINTS 14

2 3 1.40

3 4 1.40

4 5 1.40

5 6 1.40

6 7 1.40

7 2 1.40

1 2 1.08

10 8 0.96

12 4 1.08

14 5 1.08

13 6 1.08

11 9 0.96

8 3 1.364

9 7 1.364

ANGLES 20

harm 1 2 3 292.880 120.00

harm 1 2 7 292.880 120.00

harm 3 2 7 527.184 120.00

harm 2 3 4 527.184 120.00

harm 8 3 2 585.760 120.00

harm 8 3 4 585.760 120.00

harm 3 4 5 527.184 120.00

harm 12 4 3 292.880 120.00

harm 12 4 5 292.880 120.00

harm 4 5 6 527.184 120.00

harm 14 5 4 292.880 120.00

harm 14 5 6 292.880 120.00

harm 5 6 7 527.184 120.00

harm 13 6 5 292.880 120.00

harm 13 6 7 292.880 120.00

harm 6 7 2 527.184 120.00

harm 9 7 6 585.760 120.00

harm 9 7 2 585.760 120.00

harm 10 8 3 292.880 113.00

harm 11 9 7 292.880 113.00

DIHEDRALS 34

cos 1 2 3 4 15.167 180.00 2

cos 1 2 3 8 15.167 180.00 2

cos 7 2 3 4 15.167 180.00 2

cos 7 2 3 8 15.167 180.00 2

cos 2 3 4 5 15.167 180.00 2

cos 2 3 4 12 15.167 180.00 2

```
cos    8   3   4   5   15.167    180.00      2
cos    8   3   4  12   15.167    180.00      2
cos    3   4   5   6   15.167    180.00      2
cos    3   4   5  14   15.167    180.00      2
cos   12   4   5   6   15.167    180.00      2
cos   12   4   5  14   15.167    180.00      2
cos    4   5   6   7   15.167    180.00      2
cos    4   5   6  13   15.167    180.00      2
cos   14   5   6   7   15.167    180.00      2
cos   14   5   6  13   15.167    180.00      2
cos    5   6   7   2   15.167    180.00      2
cos    5   6   7   9   15.167    180.00      2
cos   13   6   7   2   15.167    180.00      2
cos   13   6   7   9   15.167    180.00      2
cos    6   7   2   3   15.167    180.00      2
cos    6   7   2   1   15.167    180.00      2
cos    9   7   2   3   15.167    180.00      2
cos    9   7   2   1   15.167    180.00      2
cos   10   8   3   4    9.094    180.00      2
cos   10   8   3   2    9.094    180.00      2
cos   11   9   7   2    9.094    180.00      2
cos   11   9   7   6    9.094    180.00      2
harm   2   7   3   1    4.602      0.00
harm   3   2   4   8    4.602      0.00
harm   4   3   5  12    4.602      0.00
harm   5   4   6  14    4.602      0.00
```

harm 6 5 7 13 4.602 0.00

harm 7 6 2 9 4.602 0.00

finish

VDW 10

CA CA buck 238577.00000 0.27778 1642.70000

CA OH buck 234281.83653 0.26515 1358.57930

CA HO buck 34641.62684 0.24619 187.93097

CA HA buck 53441.60614 0.27258 473.35429

OH OH buck 230064.00000 0.25253 1123.60000

OH HO buck 34017.96467 0.20861 155.42651

OH HA buck 52479.48308 0.25995 391.48313

HO HO buck 5030.00000 0.21459 21.50000

HO HA buck 7759.77641 0.24099 54.15349

HA HA buck 11971.00000 0.26738 136.40000
close

BIOGRAPHY

Mr. Somwang Sae-tang was born on September 13, 1985. He received his Bachelor Degree in Pharmacy (First Class Honours) in 2008 from the Faculty of Pharmaceutical Sciences, Chulalongkorn University, Bangkok, Thailand.